Quaternary International xxx (2017) 1–19

Contents lists available at ScienceDirect

Quaternary International

journal homepage: www.elsevier.com/locate/quaint

Implications for elastic energy storage in the Himalaya from the Gorkha 2015 earthquake and other incomplete ruptures of the Main Himalayan Thrust

Roger Bilham [a, *], David Mencin [a], Rebecca Bendick [b], Roland Bürgmann [c]

[a] CIRES and Geological Sciences, University of Colorado, Boulder, CO 80309-0216, USA
[b] Department of Geosciences, University of Montana, Missoula, MT 59812, USA
[c] Dept. of Earth and Planetary Science, Univ. of California, Berkeley, CA 94720-4767, USA

ARTICLE INFO

Article history:
Received 25 June 2016
Received in revised form
24 September 2016
Accepted 25 September 2016
Available online xxx

ABSTRACT

Rupture in the 2015 M7.8 Gorkha earthquake nucleated at the downdip edge of the Main Himalayan Thrust (MHT) near the transition from interseismic locking to aseismic creep beneath the Tibetan plateau, and propagated incompletely towards the Main Frontal Thrusts (MFT). Despite the imposition of a substantial static strain in the mid-décollement, afterslip on the MHT within a year of the earthquake had decayed to negligible levels. Earthquakes that incompletely rupture the MHT ($7 < Mw < 7.9$) have been relatively common in the past two centuries, and as a consequence heterogeneous patches of stored elastic strain must exist throughout the Himalaya similar to that emplaced by the Gorkha earthquake. We show that these patches of stored strain are not dissipated by creep or by subsequent updip earthquakes, with the possible exceptions of a sequence of moderate earthquakes to the west of the great 1950 Assam earthquake, and to the east of the Kangra 1905 earthquake. It is thus considered likely that mid-décollement strain newly imposed by the Gorkha earthquake, and other recent incomplete ruptures will be incorporated in the rupture of a future much larger earthquake. Incomplete ruptures (i.e. those that nucleate downdip but fail to rupture the frontal thrusts) appear to occur preferentially in parts of the central Himalaya characterized by relatively narrow transition regions of interseismic decoupling (<30 km downdip). Assuming uniform strain at failure these narrow zones are unable to store large amounts of strain energy compared to wide zones of interseismic decoupling. Since the transition from fully locked to a fully creeping rheology depends partly on temperature, to first order the width of the interseismic decoupling transition zone depends on the local dip of the MHT. Where the decoupling zone is narrow (25 km) moderate earthquakes ($6 < Mw < 7$) are observed to occur at intervals of a few hundred years. Where the transition zone is wide (e.g. Kashmir and Assam, 150 km) great earthquakes nucleate at long time intervals (millennia). Because the cumulative moment release of moderate earthquakes in regions of narrow seismic decoupling is insufficient to keep up with plate convergence, we conclude that megaquakes that eventually sweep through these regions are augmented by the heterogenous fossil strain of former incomplete ruptures. Because great earthquakes in the central Himalaya are inferred to nucleate from moderate earthquakes near the base of the MHT, the preparation zones of these moderate earthquakes may provide opportunities for forecasting the approach of future great earthquakes.

1. Introduction

Convergence rates in the Himalaya (Fig. 1) derived from GPS data vary from 11 to 13 mm/yr in Kashmir to 20 mm/yr in the central Himalaya to 12–23 mm/yr in Assam (Banerjee et al., 2008; Ader et al., 2012; Schiffman et al., 2013; Vernant et al., 2014; Stevens and Avouac, 2015). The uncertainties in velocities east of Sikkim are caused by differences in the computed rate of clockwise rotation of the Brahmaputra valley and Shillong Plateau (Vernant et al., 2014; Stevens and Avouac, 2015), a rate that is weakly constrained by

* Corresponding author.
E-mail address: bilham@colorado.edu (R. Bilham).

http://dx.doi.org/10.1016/j.quaint.2016.09.055

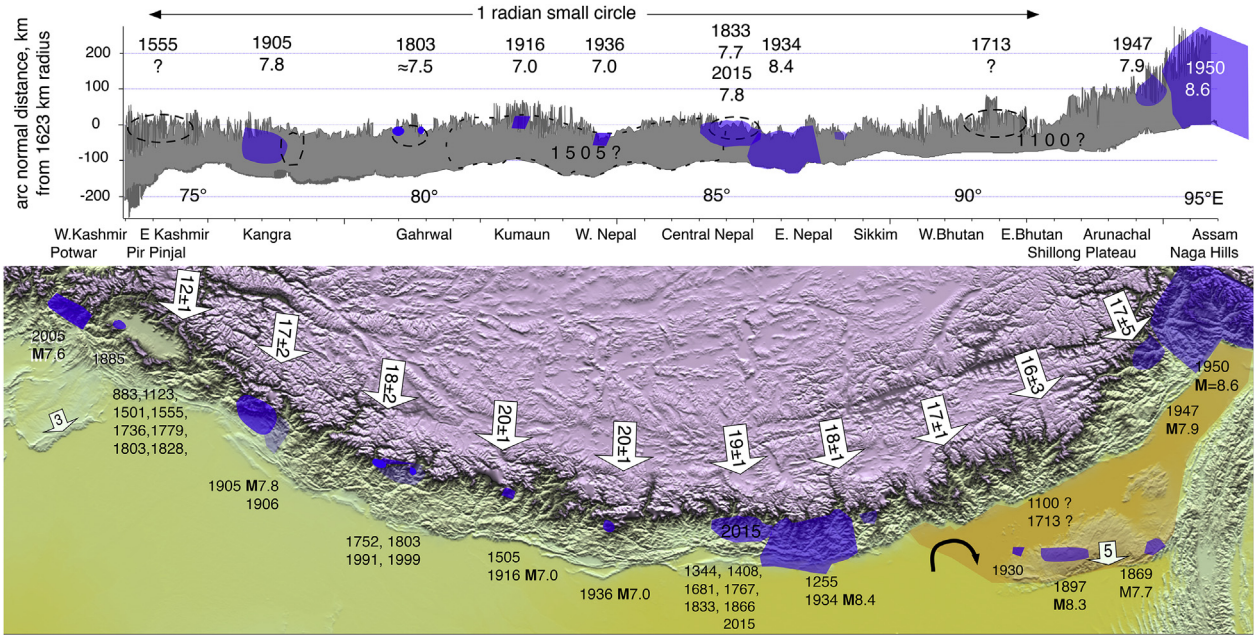

Fig. 1. Himalayan convergence velocities with rupture zones of significant historical earthquakes shaded blue. Upper plot shows the width of MHT, the region between the 3.5 km contour and the Main Front Thrust (MFT) plotted as a function of distance from a small circle radius 1623 km. Lower plot indicates inferred rupture zones of significant earthquakes in the past 200 years with magnitudes where these are well constrained. Velocities in mm/yr averaged from Vernant et al. (2014); Ader et al. (2012); Schiffman et al. (2013), and Stevens and Avouac (2015). Violet shading>3.5 km. Yellow<150 m. Clockwise rotation of the Brahmaputra valley reduces Himalayan velocities and results in convergence south of Shillong. The rupture zones of pre-1850 earthquakes are very uncertain.

currently available campaign GPS data. The Himalayan arc, as defined by the 3.5 km elevation contour (Avouac, 2003, 2015) between 77°E and 89°E approximates a small circle with radius 1623 km centered at a point near 42.10°N 90.72°E (Seeber and Gornitz, 1983; Bendick and Bilham, 2001; Vernant et al., 2014). Within this region, the arc-normal distance between the 3.5 km contour, representing the northern edge of the locked Main Himalayan Thrust (MHT) and its surface trace varies from 60 km to 110 km. Outside this 1 radian central region, in Kashmir and Assam, the width of the MHT broadens to >150 km (Fig. 1). The inferred width of the locked décollement so derived is consistent with local geodetic velocity fields determined at numerous locations along the arc (Ader et al., 2012; Banerjee et al., 2008; Schiffman et al., 2013; Vernant et al., 2014; Stevens and Avouac, 2015).

The "locking line" is a convenient term to describe the transition at depth from the fully locked part of the MHT, to its creeping downdip extension that permits India's slow aseismic descent below Tibet. However, the notion of an infinitely thin line separating the locked and freely creeping areas of the MHT, although convenient for dislocation modeling and describing the process in simple terms, in practice cannot exist (c.f. Savage, 2006). Were the line infinitely thin, the strain in the rock near the tip of this ideal discontinuity would always be close to failure due to India's 1.7 mm/month northward convergence with Tibet. No thin line of microseismicity on the plate interface is evident. Instead, microearthquakes occupy a diffuse volume many kilometers deep and tens of kilometers wide centered loosely near the 3.5 km contour (Avouac, 2003). The locking line is thus a transition zone with finite width, and appears to be so in all or most subduction zones (e.g., Bürgmann et al., 2005; Burgette et al., 2009; Chlieh et al., 2008; Hyndman, 2013). Attempts to quantify its width under the Himalaya from geodetic and seismic data have yielded values of as little as 25 km to more than 150 km depending on the location considered along the arc (Schiffman et al., 2013; Ader et al., 2012; Stevens and Avouac, 2015). In that the Main Himalayan thrust is fully locked south of this zone of partial coupling, and fully unlocked to its north, we shall refer throughout this article to this zone of incomplete seismic coupling as the *interseismic decoupling zone*.

In general, the ability of lithospheric materials to sustain seismic rupture depends on the temperature, and hence the depth of the region where tectonic slip occurs (Chen and Molnar, 1983). The finite width and depth of the interseismic decoupling zone has been attributed to a temperature dependence of the rheology on the surface of the MHT (Ader et al., 2012). At temperatures less than ≈350 °C the MHT remains locked and no slip can occur. At temperatures above ≈350 °C aseismic fault-slip can initiate, but when a small amount of slip occurs (below a critical distance, d_c), friction increases and prevents accelerated slip, that is, the fault is velocity strengthening (Marone, 1998; Blanpeid et al., 1995). At temperatures exceeding ≈450 °C, steady creep occurs. The 350 °C and 450 °C isotherms have been proposed to approximately bound the transition zone from locked to freely-slipping on subduction thrusts (e.g., Hyndman, 2013). The temperature dependent process so described (we consider an alternative process below) would result in a gradation of "seismic coupling", a transition zone where neither fully locked nor fully creeping conditions exist on the MHT. At temperatures lower than ≈350 °C seismic coupling is assigned a numerical value of unity, meaning 100% locked (seismically coupled). At temperatures higher than ≈450 °C the value is zero, meaning 100% creeping. Where the temperature of this interface is at an intermediate temperature a seismic coupling coefficient between 0 and 1 can exist. The precise temperatures where these extreme conditions occur vary with the type of materials on the interface, and with the presence or absence of fluids and metamorphic processes that we shall not consider in this article. In subduction zones, aseismic slip in and downdip of this zone is often found to occur episodically rather than by steady sliding, indicating that rate- and state-dependent frictional properties prevail (e.g., Schwartz and Rokovsky, 2007). Episodic aseismic slip has yet to be identified beneath the Himalaya.

Please cite this article in press as: Bilham, R., et al., Implications for elastic energy storage in the Himalaya from the Gorkha 2015 earthquake and other incomplete ruptures of the Main Himalayan Thrust, Quaternary International (2017), http://dx.doi.org/10.1016/j.quaint.2016.09.055

It is readily apparent that if the width of the interseismic decoupling zone is dependent on temperature, in a region of uniform geothermal gradient its width is determined by the dip of the MHT (Fig. 2). Thus if the geothermal gradient is 25 °C/km the transition from 350 °C to 450 °C occurs over a vertical depth of 4 km. Where the dip of the MHT is 6° the interseismic decoupling zone will be 4/tan6° = 38 km wide at the surface. A dip of 2° broadens the zone to 114 km. The notion of a uniform geothermal gradient is obviously too simple, given the frictional heating effects on the surface of the MHT, and by the propensity for geotherms to be modified by the downward-descending cold Indian plate (Molnar and England, 1990) or modified by the growth of duplex structures (Herman et al., 2010). This is further complicated in the Himalaya because in many locations the dip of the MHT undergoes an abrupt steepening to form a ramp close to, or as part of, the interseismic decoupling zone (Caldwell et al., 2013; Elliott et al., 2016; Grandin et al., 2015).

An alternative process for broadening the interseismic decoupling zone, that does not depend on a linearly temperature-dependent rheology is to invoke the existence of isolated strongly-coupled asperities (regions of high friction) within and near the transition zone between fully locked décollement and downdip region of aseismic creep (Bürgmann et al., 2005; Johnson et al., 2016). A relatively small locked patch within the zone of aseismic creep will concentrate strain locally thereby reducing strain in the surrounding region. Aseismic slip would thereby occur on the surrounding décollement at a reduced rate, and the surface velocity field will integrate the strain from the locked and sliding patches, effectively resulting in an interpretation of partial coupling. Bürgmann et al. (2005) show that the area of locked asperities need be relatively minor relative to the intervening areas of aseismic slip to modify the effective percentage of interseismic decoupling.

The width of the interseismic decoupling zone is important because it influences its capacity to store elastic strain energy $^1/_2 VE\varepsilon_c{}^2$ (where E = Young's Modulus, and V = volume, and ε_c is the critical strain at failure), and hence the amount of slip deficit at the moment of rupture. We illustrate the implications of dip on elastic

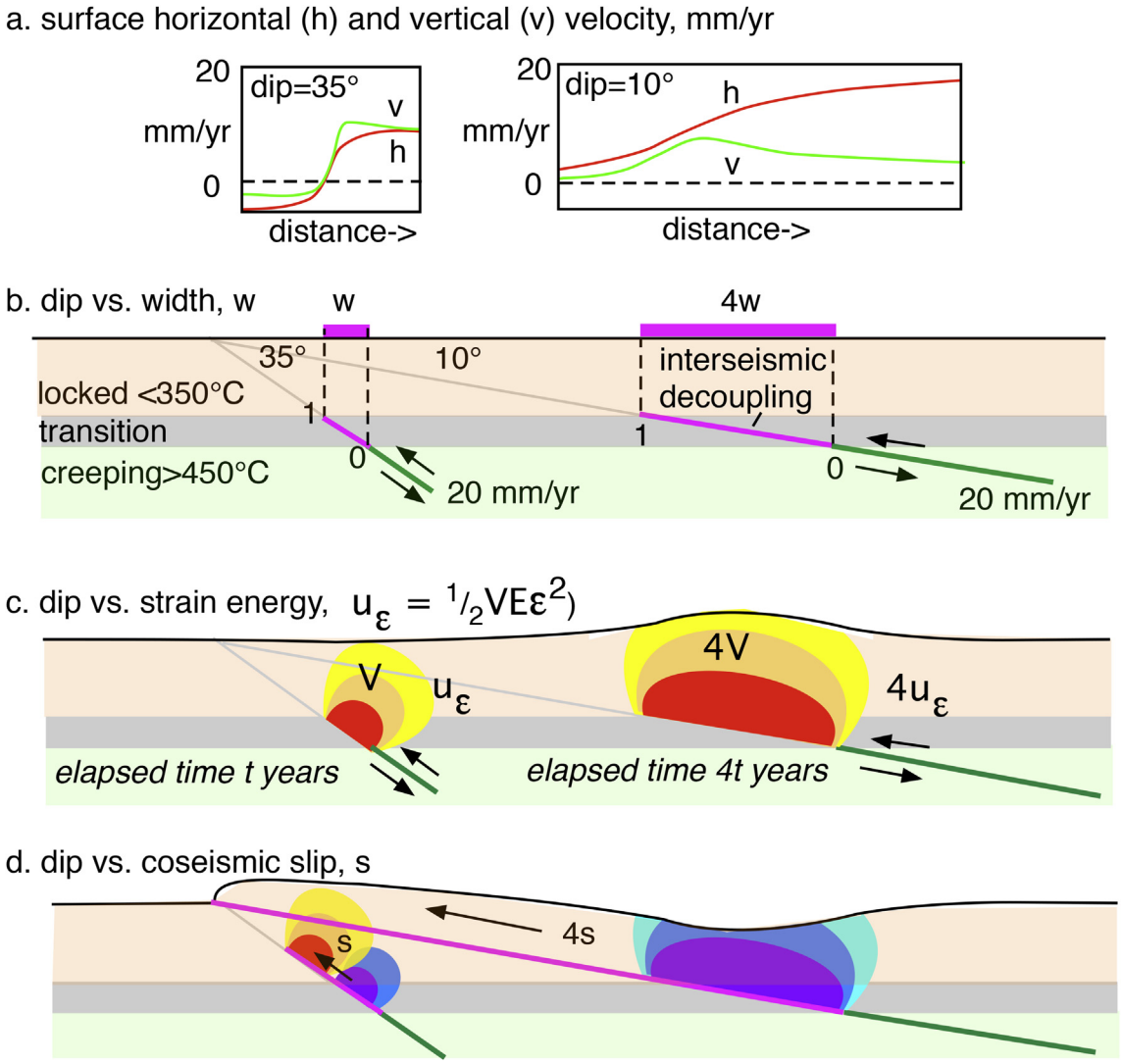

Fig. 2. Cartoon illustrating the influence of dip on (a) surface velocity fields, (b) the width of the interseismic decoupling zone, (c) the consequent increased volume (V) and capacity for this zone to store strain energy, $u_{\varepsilon\varepsilon}$ at shallow dip (E = Youngs Modulus; ε = strain), and (d) coseismic slip. The increased slip in (d) arises because a fourfold increase in time must elapse for Himalayan convergence in (c) to attain the critical strain to nucleate rupture. Thus although the strain at failure (ε_c) is the same, the slip deficit is four times greater. The grey zone in each case is the temperature-depth range within which partial interseismic decoupling occurs from 1 = fully locked, to 0 = fully creeping. Red/yellow = interseismic contraction; Blue/violet = coseismic extension; complimentary strains in the Indian plate are omitted. In the example shown (d), the shallow dipping fault has sufficient slip-potential to rupture to the surface whereas the steeply dipping fault incompletely ruptures the décollement.

Please cite this article in press as: Bilham, R., et al., Implications for elastic energy storage in the Himalaya from the Gorkha 2015 earthquake and other incomplete ruptures of the Main Himalayan Thrust, Quaternary International (2017), http://dx.doi.org/10.1016/j.quaint.2016.09.055

strain storage in a temperature-dependent model of interseismic decoupling in Fig. 2. In 2b the temperature transition zone is depicted as a 4-km-thick vertical layer corresponding to a uniform geothermal gradient from 350 °C to 450 °C starting at 15–18 km depth. Dips of 35°N and 10°N are chosen for illustrative purposes, since they represent interseismic decoupling widths that differ, in round numbers, by a factor of 4. The interseismic convergence rate in each case is identical at 20 mm/yr, but the time taken for the strain to reach critical failure, (ε_c, i.e. sufficient to nucleate rupture) is four times longer for the shallow-dipping fault, because strain is distributed within a volume four times larger downdip. As a result, when rupture occurs, the strain energy is four times larger than the strain energy for the more steeply dipping fault, and hence coseismic slip is potentially 4 times larger.

Observed GPS convergence vectors are not ubiquitously arc normal (Fig. 1) and in places an oblique component of slip, especially near the Himalayan syntaxes, results in an increase in the width of the interseismic decoupling zone in the direction of slip. This increased downdip width results in an additional increase in capacity to store strain energy, and hence potential slip during rupture in a great earthquake when it is released.

A consequence of these geometrical relationships (Fig. 2) is that if Young's Modulus and ε_c, the critical strain at failure, are uniform along the Himalayan arc we should anticipate a simple relationship between the magnitude of earthquakes and the dip of the MHT where these earthquakes nucleate. Where the dip is steep we should expect to find frequent moderate earthquakes associated with minor slip, consistent with the brevity of the short interval of interseismic convergence, and hence limited slip potential. These moderate earthquakes are likely to be associated with slip of less than a few meters and thus may incompletely rupture the MHT. Where the dip is gentle we should expect to find infrequent great earthquakes whose consequent large slip may potentially rupture the entire width of the MHT and the Main Frontal Thrusts (MFT). In a later section we compare this conclusion with what we currently know of Himalayan earthquakes.

We note that in the Gorkha earthquake the region downdip from the interseismic decoupling zone did not participate in significant coseismic strain release. Although afterslip occurred in this region, in the year following the earthquake it amounted to less than 1% of maximum coseismic slip. or 2% of the mean slip (Mencin et al., 2016).

1.1. Strain at failure

The following section emphasizes elastic strain, rather than stress, because strain is directly observable using geodetic methods. When a rock is compressed beyond its elastic limit it either ruptures or flows. Below this limit it will return to its former shape when the stress is removed. From the observation that the geodetic convergence rates observed in the central Himalaya are almost identical to the geological advance of the Himalaya over the Indian plate (Lyon Caen and Molnar, 1985; Wesnousky et al., 1999; Lavé and Avouac, 2001) we conclude that the rocks of the Himalaya are exposed to stresses below their elastic limit prior to rupture of the MHT. A minor amount of strain (<10%) appears to be converted into inelastic deformation (Stevens and Avouac, 2016). If we knew the value of the strain in the rocks at the moment of failure (ε_c), and the volume in which this strain were stored (V), we could calculate the maximum slip that would occur in the ensuing earthquake. This is the basis of the slip-predictable model for forecasting the slip in future earthquakes. Several different methods for estimating strain at failure are described, although we note that the strain required to initiate rupture nucleation in large earthquakes often eludes precise quantification, because most of the methods we describe yield an average value for the strain drop or stress-drop measured in the earthquake.

An approximate value for the strain at failure in the Gorkha earthquake can be obtained if we assume that the 2015 Mw = 7.8 earthquake was a repeat of a Mw ≈ 7.7 earthquake that occurred in 1833 (Mencin et al., 2016 (supplementary information); Bollinger et al., 2015). If we apply a definition of the strain at failure that follows from the observed ratio of coseismic slip to fault length, which for thrust earthquakes is typically $\approx 2 \times 10^{-5}$ (Scholz, 1982, 2002; Shaw and Scholz, 2008), and using the maximum slip in the earthquake (7 m) and the along-strike length of the rupture (150 km) we obtain $\varepsilon_c = 4.7 \times 10^{-5}$. Using the mean slip we obtain half this value, 2.3×10^{-5}.

A related method to estimate strain at failure is to note that the mean surface contraction rate prior to the earthquake is equivalent to a N/S contraction of $\approx 2 \times 10^{-7}$/year, a value that follows from the convergence rate of 18–20 mm/yr applied to the ≈100 km wide region above the interseismic decoupling zone. The accumulated strain at failure, assuming that this convergence rate was applicable for the past 182 years is $\varepsilon_c = 3.64 \times 10^{-5}$. This value is a minimum because it samples only the surface strain and not the strain that increases at depth close to the interseismic decoupling zone. For example if we were to use a 30-km-wide convergence zone at depth, for the same convergence rate we would obtain $\varepsilon_c = 1.1 \times 10^{-4}$.

A direct method to evaluate the strain at failure, ε_c is to use the observed surface strain in the earthquake and from this to calculate the slip distribution at depth, and from this slip distribution to calculate the total strain released. Galetzka et al. (2015) map a stress drop which varies from <1 MPa near the edges of the rupture to a peak > 6 MPa near its center, corresponding to a strain drop of 1×10^{-5} to 2×10^{-4}. The nucleation stress-drop (near the hypocenter) in the first ≈15 s was a fraction of this mean strain release (≤1 MPa) corresponding to a strain drop of 3×10^{-5}. For the 20 km radius surrounding the Gorkha hypocenter Wang and Fialko (2015) and Lindsey et al. (2015) calculate slip of 1–1.7 m corresponding to a strain of $5–8 \times 10^{-5}$. Lay et al., (2016) report the static stress drop for the Gorkha main shock as 3–3.2 MPa (strain drop $9.1–9.7 \times 10^{-5}$).

Using the source time functions from 1700 Mw > 6 earthquakes worldwide Vallée (2013) finds that the strain-drop for Mw > 6 earthquakes lies in the range 2×10^{-5} to 10^{-4} (Fig. 3). A global study of stress drop by Allmann and Shearer (2009) reported average stress drops for continental collision earthquakes of 2.6 ± 0.5 MPa (a mean strain drop of $\approx 8 \times 10^{-5}$).

These values are consistent with geodetic estimates for strain at failure reported elsewhere. Tsuboi (1933) noted that the coseismic geodetic strain ("ultimate" strain) measured in the epicentral region of Japanese earthquakes never exceeded 10^{-4}. Rikitake (1976) used Tsuboi's results and supplemented them with an additional 4 decades of triangulation and leveling data and calculated ultimate strain as $4.7 \pm 0.19 \times 10^{-5}$. In a subsequent study with additional data Rikitake (1982) reports a strain at failure for subduction zone events of $4.3 \pm 2.3 \times 10^{-5}$ and $4.4 \pm 1.7 \times 10^{-5}$ for all earthquakes. A Gaussian fit to his pre-1982 data (Fig. 3) yields a slightly lower value with larger uncertainty: $3.4 \pm 3.8 \times 10^{-5}$.

Dynamic stress drop studies of the Gorkha earthquake report values 2–3 higher than those cited above (e.g. Denolle et al., 2015; Kumar et al., 2017) attributable to the complex source time function of the rupture subsequent to nucleation (Ruff, 1999). Similarly high values are derived for dynamic stress drops for some other Himalayan earthquakes. For example Singh et al. (2002) determine stress drops of 7.7 and 6.5 MPa for the Uttarkashi and Chamoli earthquakes in the Garhwal Himalaya (strain drops of 2.3 and 2.0×10^{-4}), whereas for four Mw > 4 events in the same region

Please cite this article in press as: Bilham, R., et al., Implications for elastic energy storage in the Himalaya from the Gorkha 2015 earthquake and other incomplete ruptures of the Main Himalayan Thrust, Quaternary International (2017), http://dx.doi.org/10.1016/j.quaint.2016.09.055

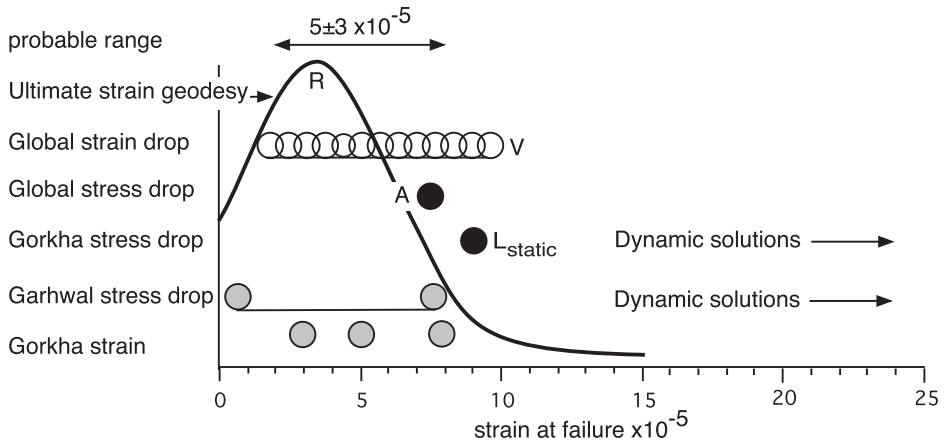

Fig. 3. Strain at failure from different methods. R = Gaussian fit to geodetic strain at failure for ≈50 earthquakes (Rikitake, 1976, 1982). V = Vallée, (2013), A = Allmann and Shearer (2009), L_{static} = Lay et al., 2016. See text for additional sources used in the figure.

Sharma and Wason (1994) report 2.5 ± 0.92 MPa. For two Mw > 3 events in this region Borkar et al. (2013) report a mean stress drop of 2.6 ± 1.8 MPa (strain drop ≈7.8 × 10^{-5}). Nearby many smaller events are associated with calculated strain drops close to 1 × 10^{-5}.

In that a chain breaks with the failure of its weakest link, the lower values for strain at failure in Fig. 3 are considered the most probable to govern initial rupture nucleation in Himalayan earthquakes. In what follows we adopt the range 2 × 10^{-5} to 8 × 10^{-5}. We recognize that stress drop is highly variable as has been demonstrated in detailed studies of earthquakes in the San Andreas system (e.g. Dreger et al., 2007; Hardebeck and Aron., 2009). We note also that our selected range strictly relates to the strain released by the earthquake, and not to the ambient absolute level of strain, which may, or may not, be equated to this release of strain.

1.2. Incomplete rupture of the MHT in the Gorkha earthquake

The 150 km × 60 km wide rupture of the Gorkha earthquake failed to completely rupture the MHT (Fig. 4), leaving a 30 km segment updip from Kathmandu unruptured (Avouac et al., 2015; Hayes et al., 2015; Galetzka et al., 2015; Bilham, 2015; Grandin et al., 2015; Duputel et al., 2016). The 70-s-duration rupture propagated from west to east as a series of sub-events, the details of which differ depending on the methods and data used. The most

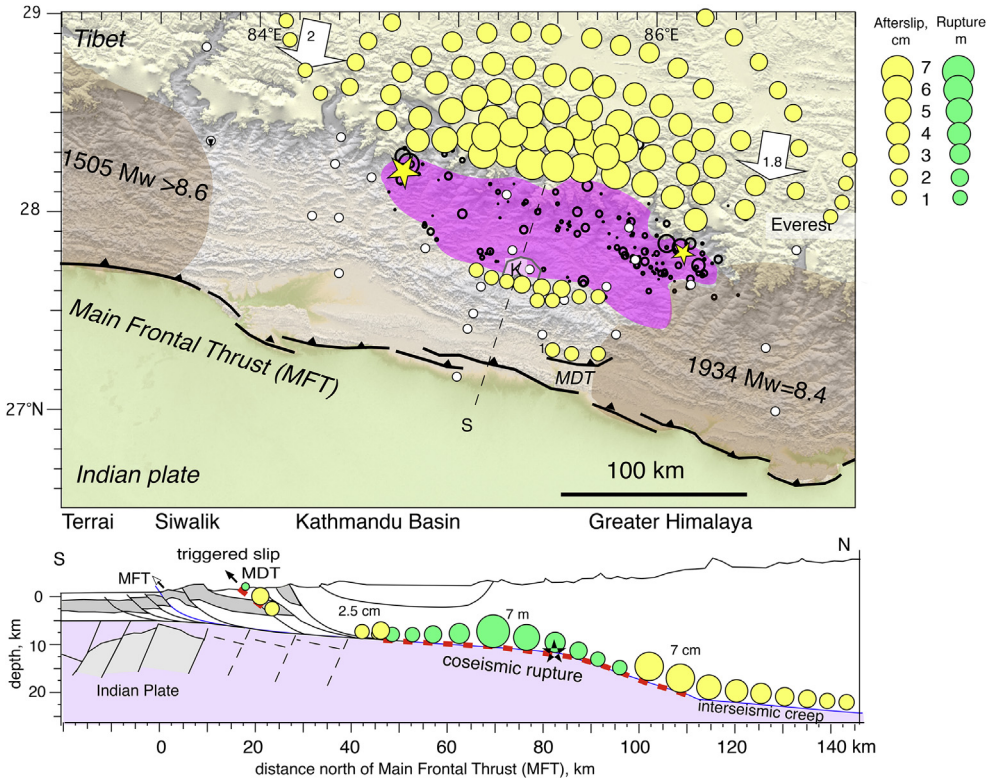

Fig. 4. The Gorkha rupture (violet) showing inferred afterslip (yellow circles scaled in cm) on the MHT six months after the mainshock, a time when 90% of the post seismic displacements were complete (Mencin et al., 2016). In the lower panel a section across the Himalaya (adapted from Elliott et al., 2016; Bashyal, 1998) is shown with coseismic slip and triggered slip on the (MDT) Main Dun Thrust (red dashed line) depicted by green circles proportional to slip in meters. Afterslip (with amplitudes ≈ 1% of coseismic slip and cumulatively equivalent to a Mw = 7.1 earthquake) is shown as yellow circles in cm. Geodetic convergence rates are arrowed in cm/yr. Black circles aftershocks, white circles are GPS points. The mainshock (WNW of the section shown) is indicated by a star.

Please cite this article in press as: Bilham, R., et al., Implications for elastic energy storage in the Himalaya from the Gorkha 2015 earthquake and other incomplete ruptures of the Main Himalayan Thrust, Quaternary International (2017), http://dx.doi.org/10.1016/j.quaint.2016.09.055

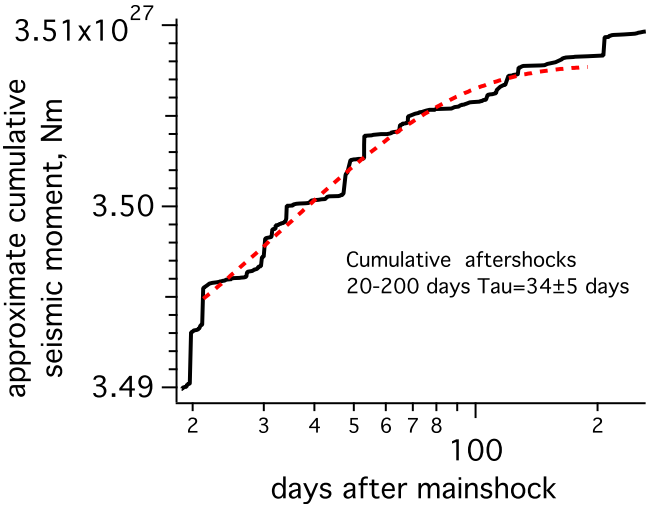

Fig. 5. The decay in cumulative moment release from aftershocks recorded for the 180 days following the Mw = 7.3 aftershock (Adhikari et al., 2015) shows a characteristic exponential decay constant of 34 ± 5 days, comparable to the 29–56 day exponential decay rates of post-seismic deformation observed by GPS receivers surrounding the rupture (Mencin et al., 2016).

insightful interpretations of the rupture process are guided by interpretation of globally distributed teleseismic data (Denolle et al., 2015). Kumar et al. (2017) interpret the rupture as four principal subevents with effective magnitudes of 7.2 < Mw < 7.4 contributing to the cumulative moment release of Mw = 7.8. In their analysis, rupture is arrested by a NNE trending strike-slip fault.

In the 6 months following the Gorkha mainshock more than 3000 aftershocks were located throughout the rupture zone and near its edges (Adhikari et al., 2015). The observed decay in cumulative seismic moment release for Mw > 4 aftershocks for the 6 months following the Mw7.3 aftershock is characterized by a decay constant of 34 ± 5 days (Fig. 5). Immediate post-seismic deformation monitored by GPS following the earthquake was relatively minor, with 5 cm of localized displacement manifest locally near its southern edge and >7 cm to the north of the rupture decaying northward (Mencin et al., 2016). The decay time constant for this deformation transient was 29–56 days (with a mean value of 43 days), comparable in duration to that indicated by the aftershocks. Aftershock moment release following the Mw = 7.3 aftershock was equivalent in magnitude to a Mw = 6.6 earthquake. Cumulative geodetically-observed post-seismic displacements during 6 months following the mainshock were equivalent in magnitude to a Mw = 7.1 earthquake, but for the same period of time shown in Fig. 5, was equivalent to a 6.9 < Mw < 7.0 silent earthquake, indicating that most of the post seismic deformation was aseismic.

1.3. Gorkha strain residual 2015

We now address the fate of the coseismic strain that occurred in April 2015 NE and NW of Kathmandu. Although aftershocks continue, postseismic deformation measurements indicate that there has been a rapid approach to the interseismic velocity field that prevailed before the earthquake. Continued slip on the MHT one year after the earthquake appears to have ceased and such strain changes as are occurring are of long wavelength and can be attributed to the viscous response of the Indian Plate. Other inelastic postseismic processes, including mantle response, can be expected over longer time scales. The destiny of the co-seismic strainfield imposed on the MHT is therefore enigmatic. Afterslip to the north continued to reduce strain associated with the deep termination of coseismic slip, whereas afterslip to the south was too limited to dissipate unruptured updip localized strain, and in any case appears to have increased loading where it did occur (Mencin et al., 2016).

Jones and Molnar (1979) note that 10% of major earthquakes are followed within 3 months and within 100 km by an earthquake with equal or greater magnitude. Clearly this has not occurred in the case of the Gorkha earthquake, but the possibility of a delayed major earthquake remains. Two historical observations in the Himalaya may be invoked to suggest that such an earthquake is unlikely in the next few years. The first is that, with one exception, no significant earthquake has followed a Mw > 7.7 earthquake in the decade following a previous major Himalayan earthquake. The second observation is that, although updip ruptures have occurred on some subduction zones (e.g. Bengkulu Mw = 7.6 in 2010, Avouac, 2015), again with one exception, we know of no historical example of spontaneous rupture of the updip shallow portion of the MHT anywhere in the Himalaya in the past 200 years.

The two exceptions mentioned in the preceding paragraph are both from Assam (93.5°E–94.5°E). In 1947, three years prior to the 1950 Great (Mw = 8.6) Assam earthquake, a Mw = 7.9 earthquake in Arunachal Pradesh (Chen and Molnar, 1977; Molnar and Deng, 1984) ruptured a region close to the westernmost edge of the 1950 rupture (Fig. 6). The 1947 rupture occurred south of the zone of interseismic decoupling defined by geodesy (Vernant et al., 2014) although the density of GPS data there are sparse and the width of the interseismic decoupling zone is presently conjectural. An unsettling conclusion from the proximity of the two ruptures is that the 1947 earthquake constituted a foreshock to the 1950 Mw = 8.6 earthquake. The possibility that it constituted a foreshock is a concern given the similarity in setting of these two earthquakes to the Gorkha earthquake and to the unruptured region to the west of the Gorkha rupture. Too little is known of the bounds of the 1947 and 1950 ruptures to support a thorough investigation of this proposition, however, it is clear that the 1947 rupture would increase Coulomb failure conditions on the MHT in contiguous regions to the east or west.

Subsequent to the great 1950 earthquake, shallow-dipping thrust earthquakes (5.4 < Mw < 6.0) occurred in 1964, 1967 and 1970 to the south of the 1947 earthquake and to the west of the inferred 1950 rupture (Chen and Molnar, 1977). No detailed field investigations of this region were undertaken and hence we are uncertain of the detailed geometry of this association. However, a plausible interpretation is that these earthquakes signify the southward progression of décollement slip on shallow updip segments of the MHT, responding to enhanced Coulomb failure imposed by the western edge of the 1950 rupture (Fig. 6). From scaling considerations the rupture dimensions of these earthquakes are too small to have completely ruptured the >80 km wide décollement updip, and we suppose that updip creep was responsible for transferring strain sufficient to nucleate updip rupture of the Mw5.4 earthquake in 1970.

Our supposition that updip rupture requires updip creep surrounding a locked asperity follows a consideration of the conditions inferred to have facilitated the mid-décollement rupture of the Kohat plateau in Pakistan on 20 May 1992. At that time, a Mw = 6 earthquake located at a depth of 8 km on the Kohat décollement ruptured a 100 km^2 patch with a dip of ≈1°N (Satyabala et al., 2012). The special conditions that led to this earthquake were attributed to southward translation of the plateau by creep at approximately 3 mm/yr, permitted by flow on the surrounding salt-rich décollement. The Arunachal décollement is unlikely to be lubricated by evaporites, and we cannot be certain that creep processes prevailed prior to the moderate earthquake

Please cite this article in press as: Bilham, R., et al., Implications for elastic energy storage in the Himalaya from the Gorkha 2015 earthquake and other incomplete ruptures of the Main Himalayan Thrust, Quaternary International (2017), http://dx.doi.org/10.1016/j.quaint.2016.09.055

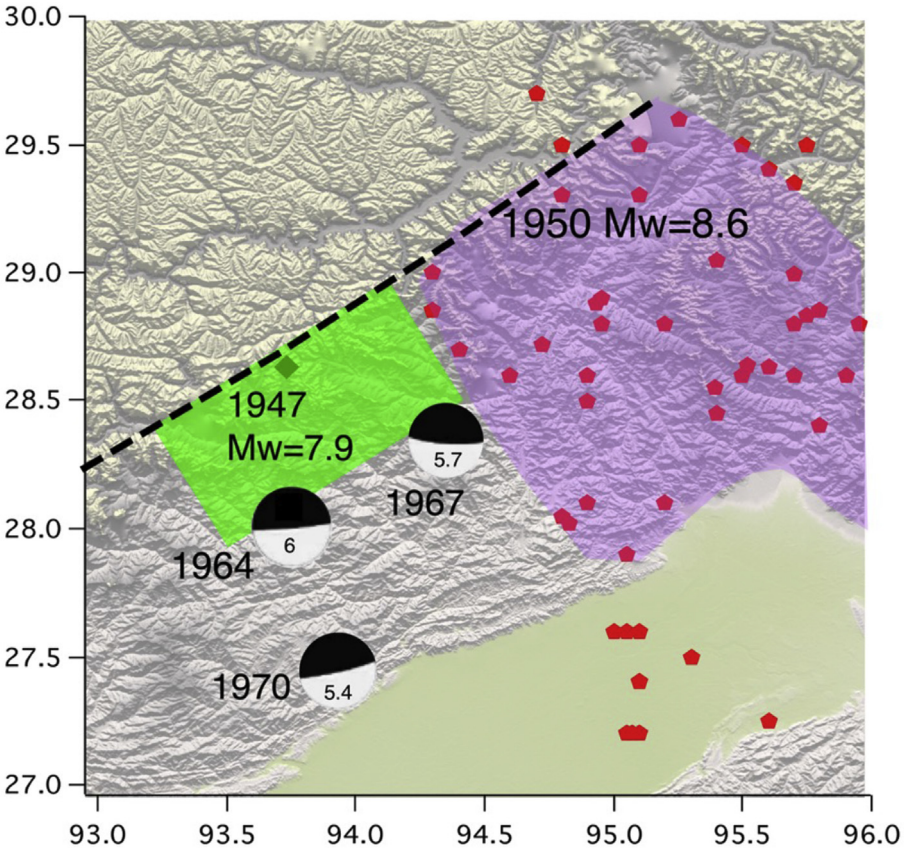

Fig. 6. The 29 July 1947 Mw = 7.9 earthquake (Chen and Molnar, 1977; Molnar and Deng, 1984) is depicted as a hypothetical 100 km × 50 km rupture zone (green) sub-parallel to the locking line inferred from GPS measurements (Vernant et al., 2013). The 1950 rupture (violet) is partly defined by aftershocks (red pentagons from Chen and Molnar, 1977). Three moderate earthquakes followed the 1947 rupture, which from their shallow depths (10–15 km) and shallow dip (3–5°N) are inferred to have occurred on the updip segment of the MHT. Focal mechanisms are from Molnar (1990) and magnitudes from the Centennial Catalog (Engdahl and Villaseñor, 2002.).

sequence depicted in Fig. 6. However, the absence of moderate mid-décollement earthquakes elsewhere in Arunachal Pradesh suggests that the sequence occurred as a result of the relief of postseismic décollement strain imposed by the 1947 and 1950 earthquakes. If this was the result of afterslip, the conditions on the Arunachal décollement must have differed from those that prevented negligible afterslip following the Gorkha earthquake.

The 1833 earthquake in Nepal resembles in many ways the recent Gorkha earthquake (Bilham, 1995; Mencin et al., 2016 (supplement)), and it is instructive to review whether any sequence of subsequent significant seismicity followed this event. No larger earthquake occurred in the decade following the earthquake, but on 23 May 1866 a $M7.2 \pm 0.2$ earthquake occurred within 80 km of the 1833 rupture, and although its mainshock location is ambiguous (Szeliga et al., 2010, Fig. 12) the scant data available for this earthquake admit a location south of Kathmandu in a similar location to a moderate earthquake in 1808, also of uncertain magnitude and location. The location of the 1866 event is weakly constrained and its probable location permits it to have occurred to the east or northeast of Kathmandu, which would correspond to the typical location of a large aftershock. Apart from the lateral uncertainty in the locations of the 1808 and 1866 earthquakes, a difficulty with pre-instrumental earthquakes is that it is often not possible to distinguish between earthquakes on the MHT from those occurring in the Indian plate at depths of 30–40 km, such as the 1987 M6.8 Udaypur earthquake, whose location at 86.5°E lies beneath the southern edge of the 1934 rupture zone (Fig. 7) and whose mechanism was strike-slip.

GPS measurements of Great Trigonometrical Survey of India (GTS) points south of the 1905 Kangra rupture reveal no significant deformation in the century following the earthquake (1905–2005) suggesting that the imposed strain from this Mw = 7.8 blind rupture was not released as aseismic slip to the south (Wallace et al., 2005; Bilham and Wallace, 2005). However, to reconcile the limited region of high intensity shaking, with the larger region of MHT slip required by the geodesy, Szeliga and Bilham (2017) needed to invoke slip to the SE of the 1905 rupture associated with a 1906 aftershock sequence. The February 1906 $6.4 < Mw < 6.8$ aftershock that initiated this sequence may have been triggered by downdip afterslip similar to that which followed the 2015 Gorkha mainshock. Modest earthquakes have occasionally occurred near the 1905 rupture but none to the south or SE (Engdahl and Villaseñor, 2002).

No major earthquakes occurred on the western or eastern edges of the 1934 Mw = 8.4 Bihar/Nepal earthquake, but on 27 May 1936 two years following the 1934 rupture, a Mw = 7.0 earthquake occurred at 83.37°E in west central Nepal (Molnar, 1990) roughly 200 km west of Kathmandu (Fig. 7). The rarity of such earthquakes suggests that its occurrence was possibly related to strain changes accompanying the 1934 earthquake, however, no unusual seismicity is known to have occurred in the intervening region west of Kathmandu.

The importance of the 1992 Kohat earthquake, and updip earthquakes that have been documented in oceanic subduction zones (e.g. the Bengkulu, Indonesia Mw = 7.6 earthquake mentioned previously) is their known association with nearby

Please cite this article in press as: Bilham, R., et al., Implications for elastic energy storage in the Himalaya from the Gorkha 2015 earthquake and other incomplete ruptures of the Main Himalayan Thrust, Quaternary International (2017), http://dx.doi.org/10.1016/j.quaint.2016.09.055

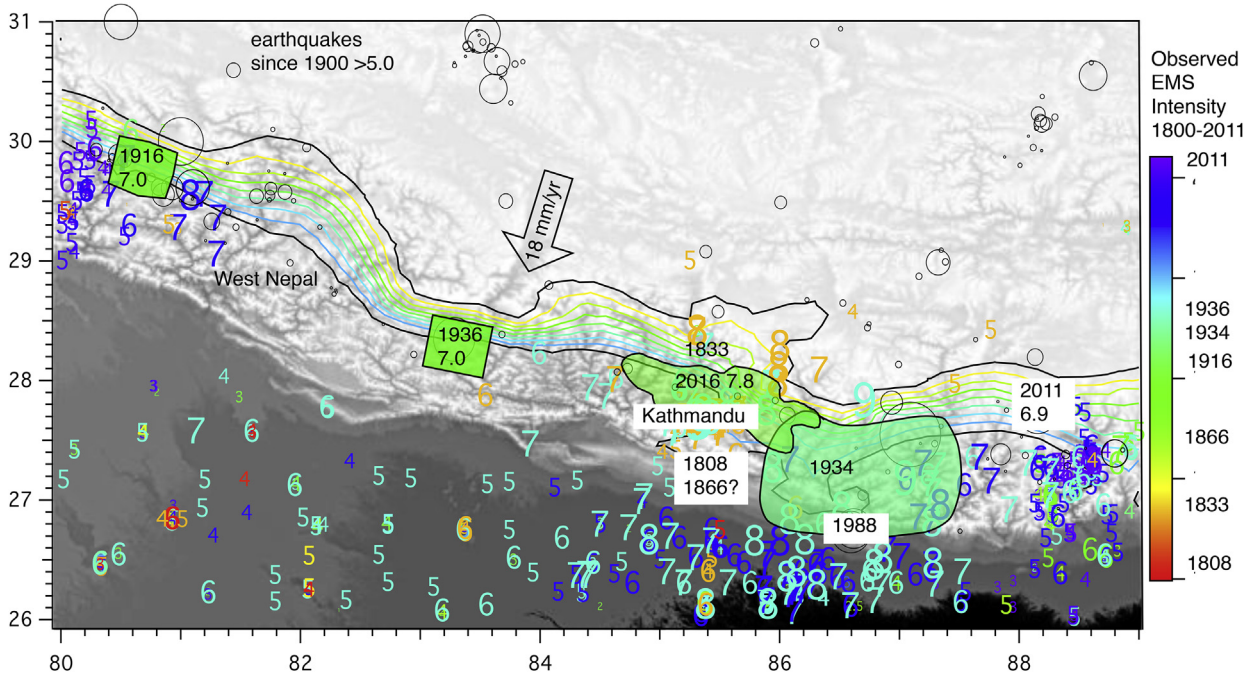

Fig. 7. Macroseismic intensity data (color coded according to date, and scaled proportional to EMS value) reported 1800–2011 (from Martin and Szeliga, 2010) indicating the locations of Mw > 5 earthquakes and approximate rupture zones of historical earthquakes. The 1988, 2011 earthquakes were strike-slip below the MHT. The locations of the 1808 and 1866 earthquakes are uncertain. Interseismic decoupling contours from Fig. 9a.

creep on the décollement. The effect of creep is to steadily, or episodically, transfer strain from downdip to updip. Without this process occurring it is apparently not possible to raise strains to levels adequate to promote thrust failure of the updip décollement.

1.4. A review of spirit leveling surveys across the Main Frontal Thrust (MFT)

No tectonic activity in the form of creep of the frontal thrusts or slow slip of the updip décollement has been reported from any of the numerous GPS surveys along the Himalaya. In contrast, leveling data from three locations along the Himalaya have in the past been interpreted as creep south of the interseismic decoupling zone (Fig. 8). In this section we question these findings.

First-order, Class-1 spirit leveling data have traditionally offered higher accuracy than vertical GPS over distances of the order of 20 km since random errors accumulate with the square-root of along-line distance, km, as $0.6\sqrt{}$km. A systematic vertical error is also present in leveling data, which is discussed below, but for distances of up to 16 km on level ground 2.4 mm accuracies are typically available, which when repeated after >10 years yield a vertical velocity accuracy of ≈0.3 mm/yr. This appealing accuracy is accompanied by a high spatial sampling of data points, and in many places by the availability of crustal deformation data preceding modern geodetic methods. In the data shown in Fig. 8 several 10–20 km wavelength features have been interpreted as evidence of slow subsurface deformation (creep) within 50 km of the Himalayan foothills.

The 130 years of vertical movements documented in the Dehra Dun region (78°E) since 1862 have been the frequently studied to investigate apparent local uplift accompanying the Mw = 7.8 Kangra earthquake (Gahalaut and Chander, 1992; 1997; Yeats et al., 1992; Gahalaut et al., 1994). Due to their proximity to the headquarters of the Survey of India, these data are sufficiently well documented to permit the identification of an unexpectedly large systematic error that escaped notice of early surveyors, or by the authors of more recent analyses. When the data for each leveling segment are plotted versus elevation, a large positive or negative correlation is evident. In first-order leveling this known slope-dependent correlation is proportional to height, as $kH \times 10^{-6}$ mm, where H is the vertical elevation traversed in meters. The constant k is typically in the range $-3 < k < 3$ for First-Order leveling with Invar staves and short symmetrical backsights and foresights, but can be much larger for wooden staves and uneven sight distances. Slope dependent errors are most pronounced on shallow gradients, rather than in steep slopes, because the error is aggravated by the leveling party adopting longer sight lines on shallow grades, where near-surface thermal gradients result in optical rays that curve more severely in the uphill direction than in the downhill direction, thereby systematically biasing the cumulative height measured. The constant k can also be influenced on steep slopes, where sight lines are usually shorter, by thermal-influences on the dimensions of the leveling rods, the scales of which in early surveys were engraved on wooden staves. Surprisingly, the value for k in the Dehra Dun leveling surveys was found to lie in the range $50 < k < 110$ north of Dehra Dun and to greatly exceed this in the gentler slopes to the south. When these correlations are removed, the 1905 earthquake (300 km to the NW) was found to have had no influence on relative elevations near Dehra Dun, consistent with the absence of shear strain in triangulation measurements near there at the time of the earthquake (Bilham, 2001). If the relative motion of the reference bench mark at Saharanpur (45 km south of the MFT) is ignored, relative motions across the Siwalik are insignificant for the period 1862–1992 (Fig. 8) suggesting an absence of creep on the southernmost MHT.

Similarly, leveling data obtained near Dalhousie (≈75.5°E) between 1960 and 1973 (Chugh, 1974) have been invoked as evidence for slip on the MHT (and MBT) south of the interseismic decoupling zone (Molnar, 1990; Gahalaut and Chander, 1999). Chugh (1974) did not publish the coordinates for Survey of India data and since the

Please cite this article in press as: Bilham, R., et al., Implications for elastic energy storage in the Himalaya from the Gorkha 2015 earthquake and other incomplete ruptures of the Main Himalayan Thrust, Quaternary International (2017), http://dx.doi.org/10.1016/j.quaint.2016.09.055

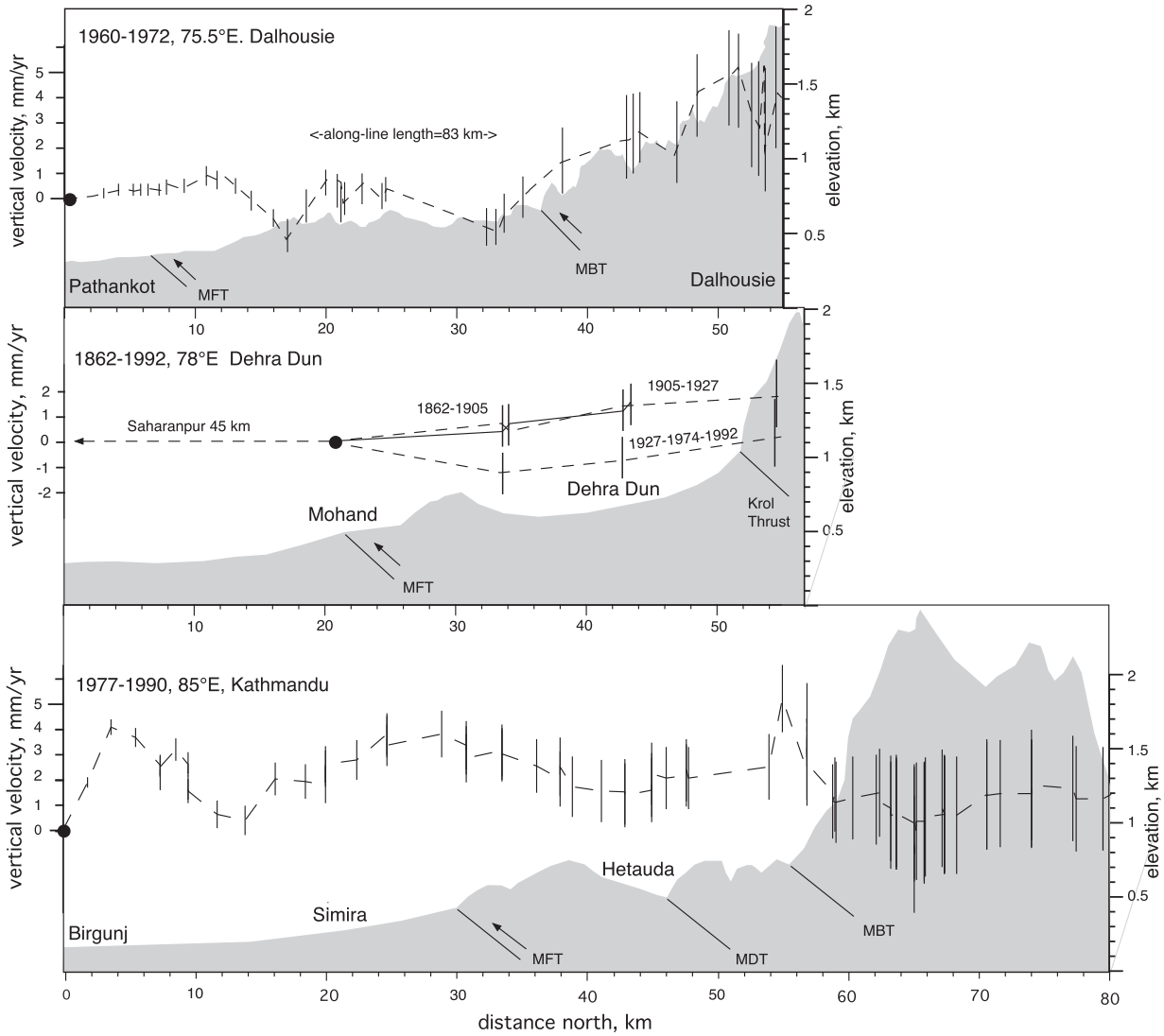

Fig. 8. Spirit-leveling data from three transects across the updip sections of frontal thrusts, where local apparent uplift has been invoked as evidence for subsurface creep (for locations see Fig. 9). A black circle indicates the starting bench mark used as the arbitrary zero datum in these plots. A 12 year interval separates the Dalhousie measurements (Chugh, 1974), five surveys in 130 years are available for the Dehra Dun segment (Bilham, 2001), and 13 years elapsed between the two Birgunj to Kathmandu surveys (Jackson and Bilham, 1994).

leveling line is 83 km long but traverses a direct distance of only 55 km horizontally, the route includes numerous hairpin ascents rendering the positions shown in Fig. 8 approximate, and thereby preventing a rigorous search for the presence of slope-dependent errors. However, between Pathankot and Dalhousie the leveling data show a weak correlation between height change and elevation, with both negative and positive polarity. If a slope-dependent error of 36 mm per vertical km is admitted in these data (twice that shown in Fig. 8a, but less than that identified in the Dehra Dun surveys), height changes in the 1960-72 data are rendered insignificant. This a much larger systematic error than accepted in first order-leveling procedures by the Survey of India (Bomford, 1928), but until the data are subjected to a critical slope analysis their presence cannot be refuted.

Finally, and crossing the 2015 Gorkha rupture, leveling surveys in 1977 and 1990 have twice connected the National leveling surveys of India and China through Nepal. The vertical-velocity in the southern half of these two surveys is plotted in Fig. 8. Although two regions of 2 mm/yr uplift were identified between the Indian border and Siwalik with wavelengths of 10 km and 20 km to the south and north of the MFT respectively (Jackson and Bilham, 1994), nearby GPS points prior to and including the Gorkha earthquake show no evidence for uplift, nor for the horizontal velocity fields needed to support published interpretations of subsurface creep on blind thrusts. A GPS control point near Simira set in silt and gravels south of the MFT currently shows weak evidence for subsidence at 1 mm/yr. This, and the absence of local horizontal deformation suggests that the origin for the leveling line, a Bench Mark at Birgunj near the Indian border, may itself be sinking at 2 mm/yr. Deep tube wells provide water for Birgunj and the potential exists for local subsidence induced by groundwater extraction.

In summary, there are a number of reasons for doubting the significance of local uplift and subsidence indicated by leveling data near the MFT, and although it is difficult to prove that they should be assigned larger measurement errors than typically associated with first-order leveling procedures, where these tests have been made they have been shown to cast doubt on claimed accuracies. We conclude that leveling data do not prove that updip creep

Please cite this article in press as: Bilham, R., et al., Implications for elastic energy storage in the Himalaya from the Gorkha 2015 earthquake and other incomplete ruptures of the Main Himalayan Thrust, Quaternary International (2017), http://dx.doi.org/10.1016/j.quaint.2016.09.055

exists, and that since GPS data from nearby regions do not require updip creep, we are justified in ignoring the leveling data.

However, shallow post-seismic creep processes may have occurred between 93.5°E and 94.5°E, and near 77°E, where GPS coverage is currently sparse (Fig. 6) and where no leveling data are available. A sequence of four earthquakes occurred 1947–1970 with shallow dip and shallow depth suggesting they all occurred on the MHT and that they progressively ruptured updip. Satyabala et al. (2012) argue that mid-décollement thrust earthquakes are unexpected due to the difficulty in transmitting stresses updip, but can be explained if creep on the surrounding décollement occurs. The 1905/6 and 1947/1970 sequences are suggestive of décollement creep and afterslip processes as discussed by Hetland et al. (2010). The MHT near 94°E may have responding to coseismic strain from the 1947 Mw7.9 and 1950 Mw = 8.6 ruptures, although direct measurements of afterslip are unavailable. Similarly, Szeliga and Bilham, (2017) argue that the 1906 earthquake near Simla may have been responsible for updip slip near 76.7°E in the year following the 1905 Kangra earthquake, as suggested by geodetic data and aftershocks.

1.5. Heterogeneous strain common throughout the Himalayan décollement

Five examples of incomplete downdip rupture in Mw = 7.5 earthquakes have occurred in the past two centuries: 1803 Garwhal, 1833 Nepal, 1905 Kangra, 1947 Arunachal, and the 2015 Gorkha earthquake in Nepal. The 1803 and 1833 rupture areas are less well defined than the three more recent events, but in this same time interval many smaller earthquakes have occurred that have also failed to rupture the MFT. For few of these earthquakes do we have sufficient knowledge of their rupture parameters to model the details of their slip, and resulting relict strain, and for pre-instrumental periods we do not know whether they rupture the MHT or other faults. For the subset that ruptured the downdip MHT we face the prospect of there being numerous hidden reservoirs of elastic strain throughout the Himalaya. They are “hidden” because they are apparently not evolving and thus remain invisible to geodesy. They are elastic in that the long term advance of the Himalaya over India is almost identical to the present day geodetic convergence rate between Indian and southern Tibet (Molnar, 1990; Avouac, 2015), with a minor inelastic contribution resulting in uplift and folding in the Himalaya (Stevens and Avouac, 2015, 2016). Since they are elastic they must eventually be released as slip on the MHT, and since this apparently does not occur as creep, and apparently does not occur spontaneously (the historical absence of updip ruptures), it must be released during future earthquake ruptures. We surmise that this invisible strain will supplement transient strain released by a future earthquake nucleating from the interseismic locking zone (Mencin et al., 2016), possibly fueling a great earthquake. We now relate the concept of ancestral strain fueling future great earthquakes, to the nucleation geometries discussed in the first part of this article.

1.6. A geometrical basis for Himalayan seismic hazards

We concluded earlier that, in a region of uniform geothermal gradient, the dip of the descending MHT controls the width of the interseismic decoupling zone, and that this in turn controls its capacity to store strain energy in the form of a slip deficit arising from tectonic convergence. With the additional assumption that the strain at failure is uniform along the Himalayan arc (for which evidence is admittedly inconclusive), this leads to the hypothesis that the width of the transition zone of interseismic decoupling controls both the inter-event time and the maximum magnitude of earthquakes that may nucleate in that segment. The implications of this conclusion are of considerable importance for seismic hazard studies in the Himalaya. A test of these implications would be to establish either a link between maximum earthquake slip and local dip, or alternatively a link between earthquake slip and the inferred width of the zone of interseismic decoupling.

Mahadevan et al. (2010) develop a theoretical framework for subduction zones that shows that a descending arcuate plate will dip more steeply in the center of its arc than near the syntaxial cusps at its extremities. This finding is consistent with the general geometry of the subsurface Indian plate. A first-order indication of the mean dip of the MHT is obtained from the width of the décollement (Fig. 1) and the difference in depth of the Indian plate beneath the MFT (≈4 km) and its depth near the interseismic decoupling zone (≈18 km). The dips so calculated vary from 4° near the syntaxes to approximately 10° in the central Himalaya, but take no account of the geometry of the complex ramp structures that define the MHT beneath the Himalaya, which may in practice determine the dip of the MHT at the critical point where it enters and passes through the interseismic decoupling zone. This geometry is known to be far from uniform, and is constrained in relatively few transects along the arc (Berger et al., 2004; Hubbard et al., 2013). In the western Himalaya (Kashmir) dip is gentle but is poorly resolved by seismic reflection profiles (Kaila et al., 1984). In other parts of the Himalaya it is defined in places by seismic reflection profiles and by receiver function profiles (Hauck et al., 1998; Alsdorf et al., 1998; Schulte-Pelkam et al., 2005; Mitra et al., 2005; Nábělek et al., 2009; Acton et al., 2011; Mahesh et al., 2015; Caldwell et al., 2013). The mean dip of the MHT in Bhutan is low (Le Roux-Mallouf et al., 2015), as it is in Assam where it can be inferred from the low morphological slope of the Himalaya assuming it to be a critical tapered wedge. These transects are too sparse to map the dip of the Himalaya along-strike although they provide a spot check of dip obtained from other methods.

The density of Mw > 5.5 earthquakes along the Himalaya in the past half-century for which routine focal mechanism solutions are available is not only sparse but samples numerous non-décollement earthquakes (Ni and Barazangi, 1984). The scattered dips evident in Fig. 9a arise both from the earthquakes near the interseismic decoupling zone that favor rupture of steeply dipping planes, and from earthquakes on ramps close to flats. The dips recorded by coseismic ruptures may be very different from the dip on which interseismic decoupling occurred prior to these earthquakes.

In the absence of a detailed “dip map” for the MHT near the location of the interseismic decoupling zone, either from geological or seismic or active source studies, we examine the width of the zone of partial seismic coupling (Fig. 9b) calculated by Stevens and Avouac (2015). Their study is important because it provides the first glimpse of the interseismic decoupling zone of the Himalaya from west to east using both GPS data and microseismicity to quantify its width and location. The Laplacian smoothing necessary to interpolate between regions where GPS data are sparse necessarily results in uncertainties that tend to broaden the zone of interseismic decoupling.

In Fig. 9b we artificially impose zero slip (seismic coupling = 1.0) near the frontal thrusts of the Pir Pinjal, Kishtwar and Uttarkhand Himal where we argue above that leveling and triangulation data do not support the presence of updip creep. Our modified map retains the general features of interseismic decoupling, including several patches of calculated updip creep in regions where GPS data are relatively abundant, but where diffuse seismicity in Stevens and Avouac (2015) study suggested a southward broadened zone of interseismic decoupling. We next contour the interseismic decoupling region to quantify its inferred width along strike. This

Please cite this article in press as: Bilham, R., et al., Implications for elastic energy storage in the Himalaya from the Gorkha 2015 earthquake and other incomplete ruptures of the Main Himalayan Thrust, Quaternary International (2017), http://dx.doi.org/10.1016/j.quaint.2016.09.055

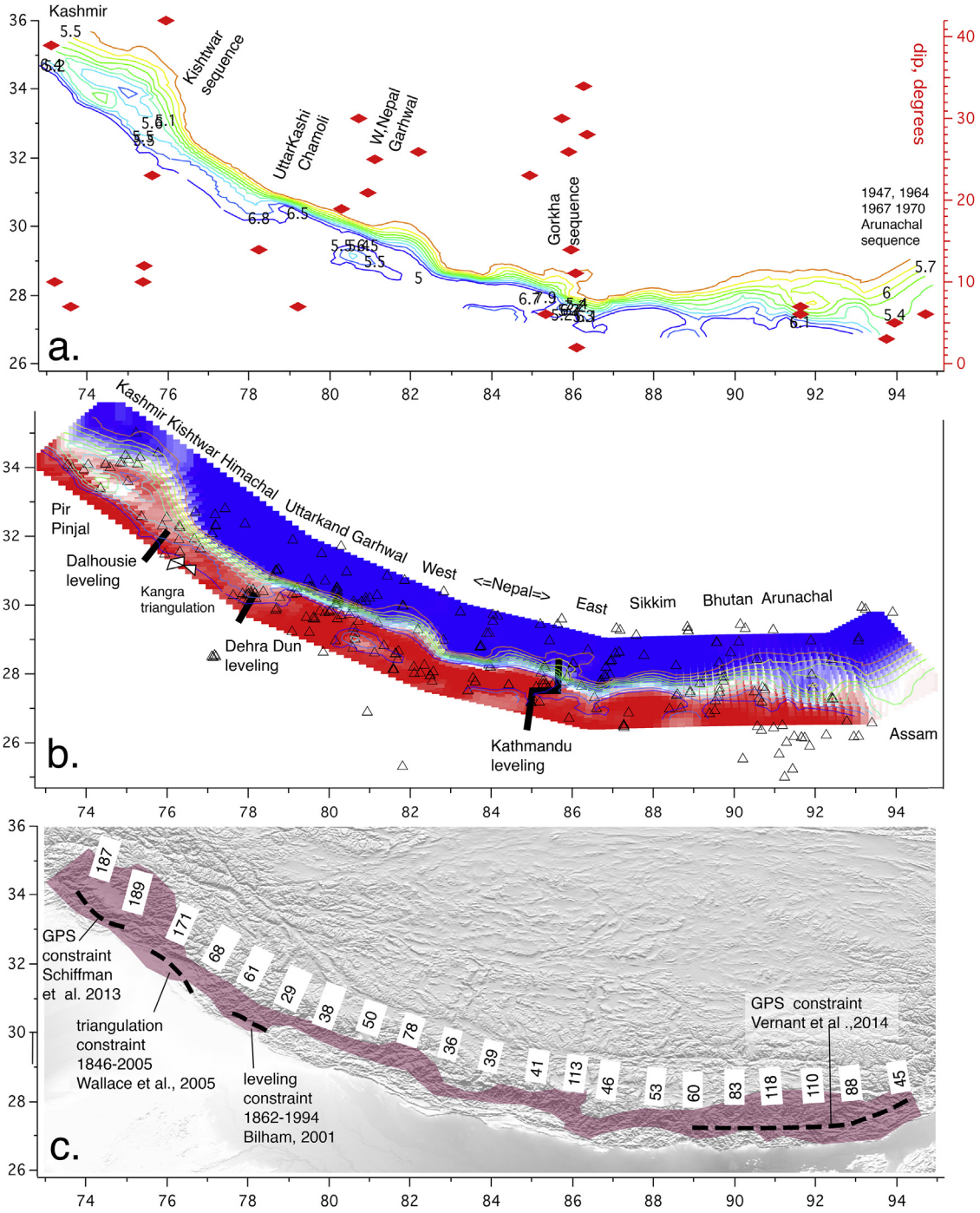

Fig. 9. **9a**. CMT-derived dips (red diamonds) for the region close to the interseismic decoupling zone 1960–2016, with locations and magnitudes of corresponding earthquakes, and interseismic decoupling contours derived in center panel. **9b**. Interseismic coupling (red locked, blue creeping modified from Stevens and Avouac, 2015). The region near the frontal thrusts west of Uttarkhand is constrained to be locked and from this modified decoupling map, contours are linearly interpolated as shown in 9a. Labeled leveling lines are those discussed in Fig. 8. Open triangles are GPS sites used by Stevens and Avouac (2015) to derive the width of the zone interseismic decoupling. **9c**. The interseismic decoupling zone from 0.9 to zero coupling is shaded, and dashed lines indicating alternative southern limits to interseismic decoupling are based on the cited analyses. White boxes indicate the width of the zone of interseismic decoupling zone in km, measured in the mean direction of local GPS vectors. Black dashed lines indicate additional southern limits to the locked MHT used to modify Stevens and Avouac (2015).

introduces additional smoothing but highlights a counter-intuitive overlap of partial seismic coupling with the MFT in places. These contours are shown in Fig. 9a and are used in Fig. 9c to shade the resulting interseismic decoupling area between 90% locked to 0% locked. In Fig. 9c we ignore isolated patches of inferred incomplete locking, for reasons discussed below related to stagnant strain and microseismicity. Finally, we invoke leveling studies that suggest that the southern limit of interseismic decoupling depicted in Fig. 9c very probably lies to the north of the interpolated contour depicting the 90% coupling at the east and west ends of the arc. This alternative southern limit to partial decoupling is indicated by a dashed black line. The width of the zone of seismic decoupling so

Please cite this article in press as: Bilham, R., et al., Implications for elastic energy storage in the Himalaya from the Gorkha 2015 earthquake and other incomplete ruptures of the Main Himalayan Thrust, Quaternary International (2017), http://dx.doi.org/10.1016/j.quaint.2016.09.055

derived varies from 189 km to 29 km (Table 1 and Fig. 10). These values are conservative estimates compared to those that would be derived from the wider zones of interseismic decoupling by Stevens and Avouac (2015) near the ends of the arc.

In Table 1 and Fig. 10 we compare the slip in earthquakes along the arc predicted from the local width of the interseismic decoupling zone, with observed slip derived from earthquakes since 1900. The instrumental data available include the Kangra Mw7.8 1905, Bhutan Mw 7.9 1947, Nepal Mw = 8.4 1934 and Assam Mw8.6 Assam 1950 earthquakes, for which mean slip remains uncertain and for which we have assigned a range of slip (Fig. 10). The slip in paleoseismic ruptures exhumed in trenches across the MFT is currently available for only ten of the 23 degree-bins we consider along the arc. However, the median slip for these is 16 m, with a mean value of 13 ± 7 m, significantly greater than the predicted slip (Fig. 10a). Few of the observed values for maximum slip on the MFT (39%) lie within the shaded area that we consider permitted by the extremal values for slip at failure, and half exceed predicted values by more than a factor of two. Thus to explain the paleoseismic slip data we would need to invoke a much higher failure strain. A plot of maximum observed slip versus predicted slip indicates that in a statistical sense the instrumental data favor a failure strain similar to that predicted (dashed line in Fig. 10b indicates a failure strain of 5×10^{-5}. In contrast a least squares fit to the paleoseismic data favors a failure strain of $1.3 \pm 0.3 \times 10^{-4}$. We argue above that this high value for strain at failure is unreasonable (Fig. 3).

However, if we compare predicted slip with observed or estimated coseismic slip in recent earthquakes (red bars in Fig. 10) we obtain good agreement with predicted slip, and the data favor the lower bounds of our estimates for strain at failure. We next examine specific segments along the arc. Consider first the segments including degrees 78°E and 79°E (Fig. 11) in the west-central Himalaya. Coseismic slips in the Uttarkashi and Chamoli earthquakes were ≈1.5 m and ≈1 m respectively (Joshi, 2006; Cotton et al., 1996; Xu et al., 2016; Thakur and Kumar, 2007), compared to minimum anticipated slip of 1.2 m and 0.6 m in Table 1. If we suppose the 1803 Garhwal earthquake at 79°E was 7.3 < Mw < 7.5 with a 40 km × 40 km rupture area it would have slipped approximately 2–4 m, approximately the amount slip that has developed since then, and within the range of anticipated slip (0.6–2.4 m). Similarly slip in recent 6.5 < Mw < 7 earthquakes for longitudes 80–81°E are consistent with the minimum anticipated slip in these regions.

In the 76°-77°E segment, slip in the 1905 Mw = 7.8 Kangra earthquake is inferred to have been ≈1.1–5.0 m (Szeliga and Bilham, 2017), whereas predicted slip budgets are 3–14 m at 76°E, and 1–5 m at 77°E near its large 1906 aftershock. Between 84°E and 85°E, at the longitudes of the Gorkha 2016 mainshock, maximum anticipated slip is 3.1–3.3 m whereas the mean slip in the earthquake was 3.5 m. Using scaling laws, slip in the Mw = 7.0 1936 Nepal earthquake would have been 1–2 m (Fig. 7) and the slip potential at 83°E is inferred to be 0.7–2.9 m. Similarly slip in the 1947 Mw7.9 earthquake would have been ≈5 m unless its rupture dimension were greater than those shown in Fig. 6. Predicted slip here is 1–7 m. Mean slip in the Great Assam earthquake is unknown but probably exceeded the predicted 5 m of synthetic slip given its large rupture area.

For some earthquakes the agreement is poor. At longitudes embracing the 1934 Mw = 8.4 earthquake anticipated slip is 2–9 m whereas mean slip in the earthquake is inferred to have been 14 m (Sapkota et al., 2013). The Riasi thrust fault near the base of the Pir Pinjal south of the Kashmir Valley has no evidence for an earthquake more recent than 4500 years ago, but its long term slip rate is 6–7 mm/yr (Gavillot et al., 2016). It is thus inferred to have a present day slip potential >27 m, significantly greater than the 15 m maximum predicted slip in Table 1.

2. Discussion

Mugnier et al. (2013) noted that the dip of the MHT controls the downdip width of the brittle/ductile transition, and highlight the diversity of rupture configurations that have nucleated near there in the past several hundred years. Stevens and Avouac (2015) note that the width of the interseismic decoupling zone determines the stressing rate. We relate this to the strain rate and hypothesize that a relation exists between the dip of the MHT, and hence the width of the zone of interseismic decoupling, and its capacity to store elastic strain. This in turn dictates the maximum slip and hence the potential magnitude of an earthquake in that segment, since shallow dips are associated with a larger storage volume, and increased slip at the moment of failure (Fig. 2). By implication, these regions of shallow dip as a consequence of their slower approach to the critical strain at failure, have longer renewal times.

Attempts to quantify these relations directly from the measured dip of the MHT near the decoupling zone are challenging because insufficient precise dip data are available along the arc (Fig. 10a), and because those that are available from focal-mechanism solutions sample the diversity of mechanisms discussed by Mugnier et al. (2013). Attempts to test this relation against the maximum slip observed in paleoseismic trenches using the published interseismic decoupling-width of Stevens and Avouac (2015) and assumptions about uniform strain at failure, in general, indicate that observed paleoseismic slip is much larger than anticipated from the mapped width of the interseismic decoupling zone, but this could

Table 1
Width of decoupling zone (km) and predicted slip (m) for strain at failure for 1° segments along arc from 73°E to 84°E and from to 84°E to 95°E. The maximum slip recorded in paleoseismic trench investigations in each degree of arc is listed in row 5 of each half of the table. For comparison purposes values for slip (m) are listed for low (2×10^{-5}) and high (8×10^{-5}) anticipated values for strain at failure.

Longitude	73°E	74°E	75°E	76°E	77°E	78°E	79°E	80°E	81°E	82°E	83°E	84°E
width, km	135	187	189	171	68	61	29	39	50	78	36	39
2×10^{-5}	2.7	3.7	3.8	3.4	1.3	1.2	0.6	0.8	1.0	1.5	0.7	0.8
8×10^{-5}	10.8	15.0	15.1	13.7	5.5	4.9	2.4	3.1	4.0	6.2	2.9	3.1
$Trench_{max}$(m)	–	–	9,27	16	16	18	26		18	8		
source	–	–	M,G	P	K	K	K		Y	H		

Longitude	84°E	85°E	86°E	87°E	88°E	89°E	90°E	91°E	92°E	93°E	94°E	95°E
width, km	39	41	113	46	53	60	83	118	110	87	46	52
2×10^{-5}	0.8	0.8	2.3	0.9	1.1	1.2	1.7	2.3	2.2	1.7	0.9	1.1
8×10^{-5}	3.1	3.3	9.0	3.7	4.2	4.8	6.7	9.4	8.8	7.0	3.7	4.1
$Trench_{max}$(m)		17		6 ± 2	14				18	2.5		<8
source		L,B		N,U	K2				K2	K2		J

B=Bollinger et al., 2014; Gavillot et al., 2016; M=Malik et al., 2010; H=Hossler et al.,2016, J=Jayangondaperumal et al., 2011; K=Kumar et al., 2006; K2=Kumar et al., 2010; L = Lavé et al., 2005; P=Philip et al., 2004, N=Nakata, 1972, 1989, 1998; U=Upreti et al., 2007; Y=Yule et al., 2007.

Please cite this article in press as: Bilham, R., et al., Implications for elastic energy storage in the Himalaya from the Gorkha 2015 earthquake and other incomplete ruptures of the Main Himalayan Thrust, Quaternary International (2017), http://dx.doi.org/10.1016/j.quaint.2016.09.055

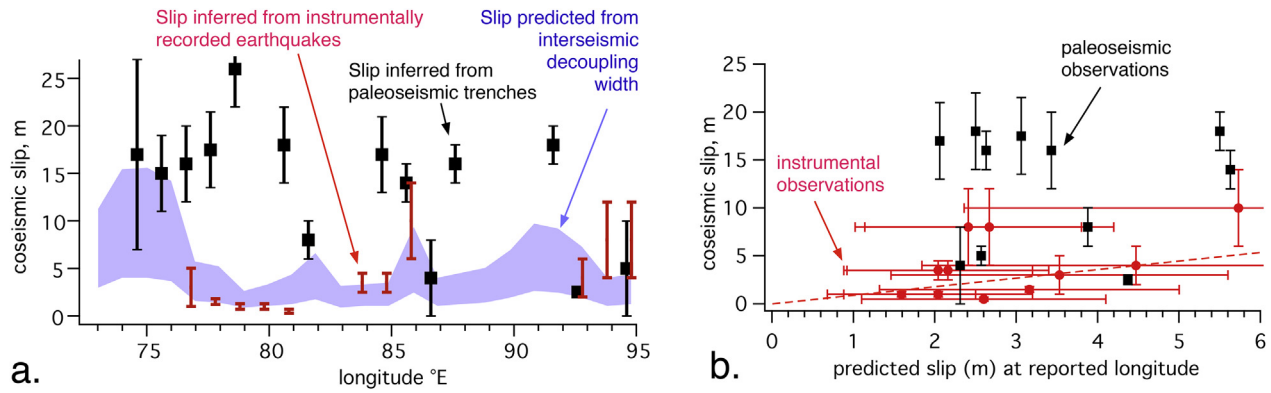

Fig. 10. **10a**. Relation between anticipated slip (violet envelope indicates failure strain of $5\pm3 \times 10^{-5}$, observed coseismic slip for recent earthquakes (red bars indicating coseismic slip uncertainty), and maximum observed paleoseismic slip (squares with estimated uncertainties) as a function of longitude. **10b**. Observed maximum paleoseismic slip exceeds predicted slip in most segments, implying a strain at failure $\geq 10^{-4}$. In contrast, slip in observed moderate earthquakes in the central Himalaya are consistent with predicted failure strains (dashed line failure strain 5×10^{-5}).

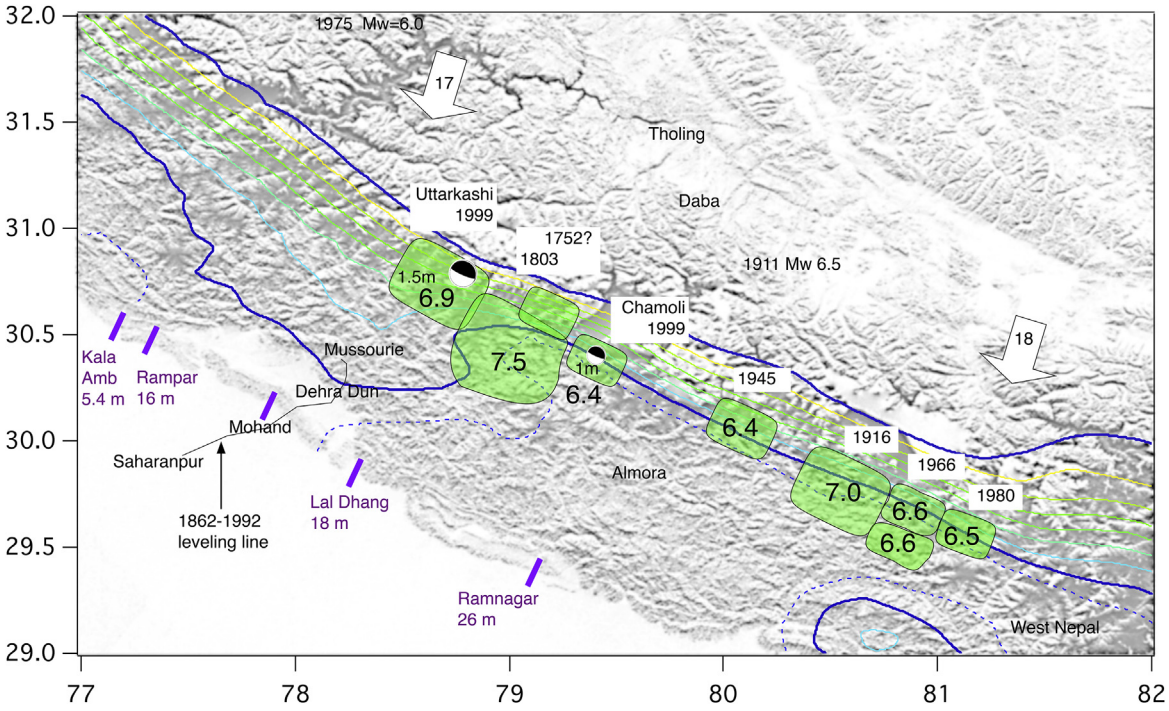

Fig. 11. Moderate Himalayan earthquakes since 1752 between longitudes 77°E and 82°E. Bold blue contours envelope the interseismic decoupling zone between 0.9 and zero coupling, dashed line = 1.0 i.e. locked (Stevens and Avouac, 2015). The 1752 and 1803 rupture zones shown are conjectural (the 1752 earthquake may have occurred close to Daba). Rupture zones for other earthquakes are scaled in proportion to magnitude. Paleoseismic trenches (violet bars) with maximum slip indicated from Kumar et al. (2006; 2010). An 8.6 < Mw < 8.8 earthquake is inferred to have ruptured the entire décollement 6 June 1505 (Ambraseys and Jackson, 2003).

arise as a consequence of the presence of incomplete ruptures in the Himalaya. A specific example is the region between 78.5°E and 81.5°E where paleoseismic trenches record maximum coseismic slips of 18–26 m, and where we predict slips of 1–5 m.

However, the recent mode of seismic energy release in these segments (78.5°–81.5°) consists of moderate earthquakes (Fig. 11) whose slip is indeed typically less than 2 m. The numerous earthquakes known in the region since 1752, include several in the instrumental period for which magnitudes and in some cases slip parameters are available. The epicenter of the 1752 earthquake, which destroyed Tholing and Daba monasteries (Ambraseys and Jackson (2003) indicate its date as 1751), may have occurred in southern Tibet and not have been a décollement event since no damage was reported from the Indian Himalaya. The 1803 earthquake has been assigned a range of magnitudes (Bilham, 2004; Ambraseys and Douglas, 2004; Szeliga et al., 2010) and its location is poorly known, but based on its macroseismic data (Dasgupta and Mukhopadhyay, 2014) it was located near the 1991 Uttarkashi and 1991 Chamoli earthquakes. We place its rupture area between the two, but caution that macroseismic data permit its rupture zone to overlap either of the two earthquakes, or even to have not been a décollement event. Even with these uncertainties, and because the renewal time for a 7.4 < Mw < 7.6 earthquake is of the order of 200 years here, a recurrence of the 1803 earthquake is currently possible. A similar unruptured area lies to the east of the Chamoli earthquake.

The continued rupture of the 79°–82° segment in moderate earthquakes, and the absence of creep processes to remove it, with

Please cite this article in press as: Bilham, R., et al., Implications for elastic energy storage in the Himalaya from the Gorkha 2015 earthquake and other incomplete ruptures of the Main Himalayan Thrust, Quaternary International (2017), http://dx.doi.org/10.1016/j.quaint.2016.09.055

one caveat, must therefore result in the incremental growth of a mid-decollement, heterogeneous reservoir of stored elastic strain. The caveat is that many minor earthquakes rupture steep reverse faults that release strain to the free surface above the décollement (Kayal, 2001). That these are insignificant in the long term comes from the approximate equality between geological advance over the Indian plate and present day geodetic convergence rates in the Himalaya (Lyon Caen and Molnar, 1985; Wesnousky et al., 1999; Lavé and Avouac, 2001; Stevens and Avouac, 2016). In the same way that the Gorkha earthquake, and presumably the 1833 earthquake before it, have incremented the strainfield in mid-decollement near Kathmandu (Mencin et al., 2016), we envisage that numerous modest earthquakes with shallow dip in the Dehra Dun/Almora segment have incremented strain on the décollement near and north of these cities awaiting a future triggering event that will permit wholesale rupture to the MFT. The June 1505 earthquake may have been the most recent event to do this (Yule et al., 2007) although we note that as yet few paleoseismic trenches have unequivocally identified its surface rupture. We envisage that moderate earthquakes have been occurring at 50–200 year intervals since 1505 or an earlier event Mugnier et al. (2013), some of which may have escaped notice in the historical record, that will have further incremented the stored strain in this region. The current slip potential in this segment is $\geq$ 10 m, some of which is "dormant" south of the interseismic decoupling zone, and some of which is being steadily incremented within the interseismic decoupling zone. We envisage that this combined stored elastic energy will fuel the next great earthquake in the region.

The process we outline extends that proposed by Mencin et al. (2016) and differs from previous views of great Himalayan earthquakes, in that hitherto it has been supposed that elastic energy used to drive great earthquakes accumulates and dissipates entirely in and near the interseismic decoupling zone. The difficulty in storing sufficient strain energy to drive great earthquakes (with>15 m of slip) in the narrow volume near a locking line was addressed by Feldl and Bilham (2006) who invoked an elastic strainfield extending northward into Tibet. The Gorkha earthquake, though Mw < 8, demonstrated that relatively modest strain was transferred from southern Tibet to the Himalaya (Mencin et al., 2016). In the model presented here the accumulation zone includes a region to the south of this interseismic decoupling region where strain is incremented episodically by moderate earthquakes and remains dormant, undetectable to geodesy, awaiting reactivation and incorporation in the rupture of a future earthquake propagating updip or along-strike.

We have thus far made no mention of along-arc segmentation that may arrest the eastward or westward growth of great earthquakes along-strike. Along-strike propagation clearly has relevance to the incorporation of latent mid-décollement strain energy once an earthquake nucleates, and the degree that it will grow or terminate laterally will depend on the previous history of moderate earthquakes in the path of the rupture propagation. Slip at the moment of nucleation thus does not determine the ultimate magnitude of the ensuing rupture. The rupture may grow in slip both updip and along strike, with associated increase in translation and surface acceleration (Bilham, 2016). It is, however, considered very probable that abrupt changes in the width of the interseismic decoupling zone along the arc signify changes in dip that may act to arrest along-arc rupture propagation (Hubbard et al., 2013). Currently, however, we consider the decoupling zone to be too imprecisely mapped to conjecture how these may have controlled the length of great historical earthquakes in the Himalaya.

We noted above that for much of the central Himalaya the magnitudes of moderate and major earthquakes (Mw < 7.9) are consistent with the currently-known width of the interseismic decoupling zone releasing strain at failure-levels of $<8 \times 10^{-5}$. The slip distribution in these earthquakes can be expected to show typically smooth central or skewed maxima, tapering to low values near the edges of their ruptures, as was observed in the Gorkha earthquake. In contrast, great earthquakes that rupture the frontal thrusts in the central Himalaya, can apparently do so only by incorporating latent strain energy inherited from former incomplete ruptures in the mid-decollement. We argue that earthquakes in this region typically release strain in the interseismic decoupling zone after only a few meters of interseismic convergence, insufficient to rupture to, and offset the MFT. The slip distributions in Mw > 8 ruptures in this region are thus heterogeneous, with maximum slip biased toward the updip portion of the MHT. As a consequence, the moment-magnitude estimates of these earthquakes are likely to be associated with inflated magnitudes, if the observed surface slip is interpreted as uniform slip throughout the rupture.

Although M > 8 earthquakes that rupture the MFT in the central Himalaya are hypothesized to incorporate the latent strain left by numerous former incomplete ruptures, the mean recurrence interval between these great earthquakes remains that calculated from the local slip deficit inferred from India/Tibet convergence. However, there are two important implications of the piecemeal release of accumulating slip deficit prior a great earthquake. The great earthquakes that are responsible for translating the Himalayan carapace southward may do so with lower magnitudes than they would, were they to release a uniform slip distribution. For example, earthquakes in c.1100, 1255 and 1505 (Mugnier et al., 2013; Mishra et al., 2016; Wesnousky et al., 2016) that were inferred to be 8.6 < Mw < 9 may have been associated with mean slip of less than half their observed maximum slip, reducing their magnitudes by 0.2 magnitude units. This additional uncertainty is currently small given the uncertainties associated with estimating the magnitudes of earthquakes inferred in paleoseismic trenches.

The second implication is that if great earthquakes nucleate from moderate downdip earthquakes, the occurrence of these moderate earthquakes may dictate the timing of future great earthquakes. For example, the 1999 Chamoli and 1991 UttarKashi earthquakes each incremented the probability for a repeat rupture of the 1505 earthquake whose slip potential was then $\approx$10 m. The future failure of Mw = 7 rupture areas near these two earthquakes (Fig. 11) will additionally increment the region toward failure in a Mw > 8.0 earthquake. Moderate earthquakes on the downdip MHT thus represent quantifiable increments in probability should operational earthquake forecasting become feasible in the Himalaya. The implication here is that the recurrence of moderate earthquakes in some parts of the Himalaya offer targets for focused earthquake monitoring experiments suited to recognizing the potential triggering of great earthquakes.

2.1. Limits to geodetic resolution?

The deformation rates in our conjectured passive strain-storage regions appear to be stagnant, or at least insufficiently active to be detectable with surface geodesy. However, the strain in these regions is likely to be the locus of weak persistent microseismicity. It is further probable that this microseismicity, though releasing negligible moment, would merge and be indistinguishable from the southern edge of the cloud of ongoing microseismicity associated with strain cycling above and near the interseismic decoupling zone. Because the present density of GPS measurements in the Himalaya is currently insufficient to define the interseismic decoupling zone uniquely, Stevens and Avouac (2015) enlisted Himalayan microseismicity to constrain the width of interseismic decoupling. By including microseismicity a wider decoupling zone

Please cite this article in press as: Bilham, R., et al., Implications for elastic energy storage in the Himalaya from the Gorkha 2015 earthquake and other incomplete ruptures of the Main Himalayan Thrust, Quaternary International (2017), http://dx.doi.org/10.1016/j.quaint.2016.09.055

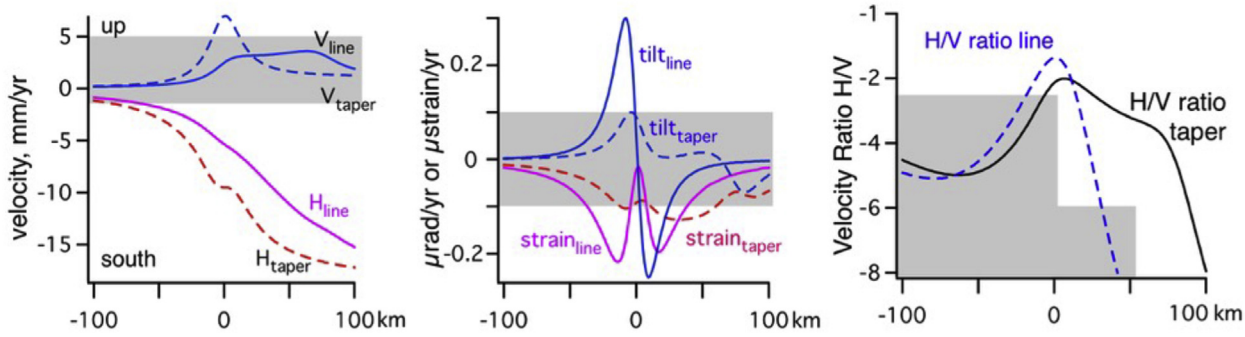

Fig. 12. Vertical and horizontal velocity fields for a planar Main Himalayan Thrust (MHT) with 3° dip. Line models result from an unrealistically abrupt transition zone, tapered models result from interseismic decoupling starting at 15 km depth leading to complete decoupling at 19 km depth. Center panel shows the strain and tilt field, and the right panel shows the ratio of GPS horizontal to vertical velocities (India fixed). Noise levels are shown as grey shading estimated for 1 year of data corrected for monsoon loading and seasonal noise. Four years of data would effectively halve the noise levels depicted.

may have been identified that includes both the active zone of interseismic decoupling, and part of the zone of dormant strain inherited from former incomplete ruptures. Distinguishing between the two has utility in seismic hazard assessment because the inherited strain is effectively invisible to surface geodesy. Our ability to distinguish these two sources of strain energy depends on signal-to-noise available in current and projected geodetic methods.

In this section we address briefly the challenge attending attempts to define the location and width of the zone of interseismic decoupling using geodetic constraints alone (e.g. Ader et al., 2012). The noise level of recent GPS data from the Himalaya indicate that a year of data, after correction for monsoon loading effects and residual seasonal signals, yields a noise level of approximately 1 mm/yr in horizontal velocities, and 2–3 mm/yr in vertical velocities (Mencin et al., 2016). Thus with 4 years of continuous data, velocity noise levels of 0.5 mm/yr and 1.5 mm/yr are possible for horizontal and vertical GPS data respectively (Fig. 12), approaching the systematic noise threshold limited by control point instability, tropospheric noise, and noise in the GPS receivers (Williams et al., 2004; Langbein, 2008). In Fig. 13 we illustrate the difference in vertical and horizontal surface velocities on a planar fault dipping at 3°, between an abrupt locking line and tapered slip for a 3° interseismic decoupling zone. The velocity fields for 20 mm/yr convergence locked for depths shallower than 15 km in each case are distinctly different, but the differences in velocity for different dip (Fig. 13) and for more complex geometries of interseismic decoupling become increasingly subtle.

In Fig. 12 differences in horizontal velocities are a factor of four above the noise. The tilt and strain signals associated with interseismic decoupling, though rich in spatial information, are close to the noise levels of long-baseline tiltmeters and strainmeters, and much below the annual noise levels of borehole strainmeters and tiltmeters. Specifically, the strain and tilt fields from elliptically tapered interseismic decoupling are too long wavelength and develop too slowly for tiltmeters and strainmeters to detect. In contrast, the ratio of horizontal to vertical GPS velocity exhibits a unique spatial distribution, which in Fig. 12 is shown in grey where the vertical or horizontal component of the derived ratio lies below its characteristic noise level.

In Fig. 13 we show the differences between surface velocities for 3°, 6° and 9° dipping planar décollements, and the surface velocity field for a 12° dipping MHT. In these models we assume that the width of the interseismic decoupling zone is proportional to dip. It is evident from these calculations that differences between 9° and 12° velocity fields cannot be distinguished, except perhaps from the distinctive variation in the ratio of horizontal to vertical slip. A 12°–9° shallowing in dip corresponds to an interseismic decoupling zone width increase from 19 km to 25 km. In contrast, the difference in width between a 6° and 3° dipping MHT is clearly above the noise level (corresponding to a width increase from 38 to 76 km). In theory, clusters of GPS measurements with a spacing of <4 km offer possible advantages in simultaneously reducing monument noise and enhancing the ability to examine north-south

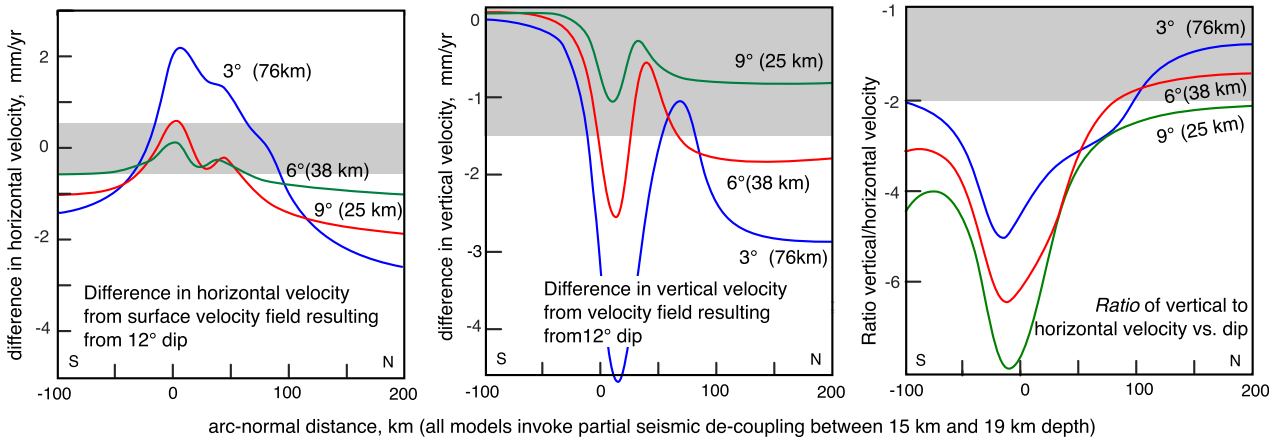

Fig. 13. Surface velocity differences between subsurface tapered slip on a planar décollement dipping at 12° from those dipping at 3°, 6° and 9°. Left = horizontal, center = vertical, and right = ratio H/V. Typical noise level appropriate for 4 years of observations are shown as grey shaded regions.

Please cite this article in press as: Bilham, R., et al., Implications for elastic energy storage in the Himalaya from the Gorkha 2015 earthquake and other incomplete ruptures of the Main Himalayan Thrust, Quaternary International (2017), http://dx.doi.org/10.1016/j.quaint.2016.09.055

gradients in strain or tilt. In theory each cluster of four would halve the noise level shown in Fig. 13 (to 0.25 mm/yr horizontal, and 0.7 mm/yr vertical, but further gains in signal to noise would appear to demand dozens of instruments in each cluster, and the absence of other forms of systematic error such as strain-tilt coupling caused by topography.

3. Conclusions

We hypothesize that the capacity of the Himalayan convergence zone to store strain energy during the interseismic cycle and hence to drive great earthquakes, depends on the downdip width of the region where strain accumulates, which we equate with the width of the transition zone of interseismic decoupling. This region lies at the base of the interseismically-locked Main Himalayan Thrust where rheological conditions favoring incomplete seismic coupling commences. Decoupling increases in degree downward until it encounters rheological conditions favoring steady creep. Elastic strain stored above this region of steady creep, in the recent Gorkha earthquake appears not to participate in coseismic rupture. We note that if seismic coupling is solely temperature dependent and geothermal gradients are uniform along the arc the resulting widths of interseismic decoupling are inversely proportional to the sine of the dip, and for anticipated dips between 3° and 20°, interseismic decoupling widths vary from 20 km to 135 km.

If we assume a uniform strain at failure for the updip edge of this strain accumulation zone, the width of interseismic decoupling determines both the slip-potential and the renewal time. Numerical estimates for the width of the interseismic decoupling zone are tabulated at one-degree intervals along the arc from the published map of Stevens and Avouac (2015), modified in places to ignore possible influence from historical leveling data of uncertain accuracy. For widths from 30 km to 130 km and for failure strains of the order of a few parts in 10^{-4} the calculated slip potential varies from ≈2 m, with a century-duration renewal times near the center of the arc, to ≈20 m with millennium-scale renewal times near the syntaxes.

Our predictions for coseismic slip are close to those observed paleoseismically near the ends of the arc. Predicted slip inferred from the width the zone of seismic decoupling near the center of the arc is generally lower than maximum paleoseismic slip on the MFT by a factor of 2–3, but is similar to co-seismic slip observed in recent moderate earthquakes. We characterize these recent earthquakes as similar to the Gorkha earthquake in that they represent incomplete ruptures of the MHT. These earthquakes include the 1991 Uttarkashi, 1999 Chamoli and 2015 Gorkha ruptures that we note have distributed strain energy within the décollement south of the interseismic decoupling zone, and also historical earthquakes in the past two centuries (1803 Kumaun, 1833 Nepal, 1905 Kangra, 1947 Assam earthquakes). The incomplete rupture of the MHT in these earthquakes suggests that a dormant heterogeneous strain field prevails through the Himalaya. We hypothesize that this dormant strain-field fuels, and is released by, occasional megaquakes that grow updip and along-strike and in so doing completely rupture the MHT. These megaquakes result in the large ruptures of the MFT in the central Himalaya recorded in paleoseismic trench investigations.

Despite their incorporation of relict décollement strain, megaquakes that rupture the Main Frontal Thrust in the central Himalaya can be expected to recur at intervals consistent with the interseismic slip that would have accrued in the absence of intervening incomplete ruptures. However, because of their enhanced updip slip distribution they will be associated with lower magnitudes than would be inferred from their surface slip and the assumption of uniform slip throughout the rupture area. Moreover, since the capacity of elastic strain energy storage in the central Himalaya is insufficient to drive the large slip recorded in 8 < Mw < 9 earthquakes, it follows that these great earthquakes must nucleate from smaller downdip earthquakes that grow along-strike and downdip. Thus the focused study of the rupture zones of future moderate earthquakes offers potential insights into the timing of great earthquakes. In some cases (75°E–84°E) we can identify candidate areas where downdip moderate earthquakes may be overdue, but throughout most of the Himalaya the historical and instrumental record is inadequate to establish patterns for the occurrence of moderate earthquakes, and such events are currently inaccessible to paleoseismic investigative methods.

Although Stevens and Avouac (2015) map of incomplete seismic coupling approximates the general dip of the leading edge of a flexed Indian plate predicted by Mahadevan et al. (2010) focal mechanisms and seismic reflection and receiver function studies that provide constraints on local dip are insufficiently dense to confirm whether inferred interseismic decoupling widths conform with a predicted relation between dip and width. We speculate that microseismicity south of the interseismic decoupling zone may in part reflect the presence of a dormant strainfield imposed by historical earthquakes. This dormant strainfield is invisible to geodesy because its rate of relaxation is slow or non-existent. In recent attempts to map the interseismic strainfield it has been necessary to incorporate microseismity near the interseismic decoupling zone to constrain regions where geodetic constraints on its width are sparse, with the possible consequence that the inferred extent of interseismic decoupling is broadened southward by its presence. In principle, a dense and uniform coverage of geodetic control points would permit the interseismic decoupling zone to be mapped independently of microseismicity and permit these active and dormant strain accumulation zones to be distinguished. We note that current GPS noise levels of 1–2 mm/yr in the horizontal and vertical limit the precision with which this can be achieved, and that the amplitude and temporal scale of strains and tilts associated with interseismic locking Himalaya are too low to be measured by borehole or long baseline strainmeters and tiltmeters.

We conclude, as do Stevens and Avouac (2015, 2016), that the width of the Himalayan interseismic decoupling zone provides a crucial role in controlling seismic hazards along the Himalayan arc. We propose that its width determines both the strain available to drive future earthquakes and the recurrence interval between them. In the central Himalaya where moderate earthquakes occur frequently, because insufficient strain energy can be stored in the interseismic decoupling zone to drive great earthquakes, those great earthquakes that occur, are fueled by latent strain inherited from ancestral incomplete ruptures.

Acknowledgements

The investigation was funded by NSF RAPID EAR1546636. We thank Peter Shearer, Marine Denolle and Peter Molnar for discussions concerning stress drop, and Vicky Stevens for providing us with a revised matrix of seismic coupling from Stevens and Avouac, 2015. Steve Wesnousky and an anonymous reviewer critically reviewed the manuscript and offered several helpful suggestions that have led to numerous improvements. We thank them both.

References

Acton, C.E., Priestley, K., Mitra, S., Gaur, V.K., 2011. Crustal structure of the Darjeeling–Sikkim Himalaya and southern Tibet. Geophys. J. Int. 184, 829–852. http://dx.doi.org/10.1111/j.1365-246X.2010.04868.x.

Ader, T., Avouac, J.-P., Liu Zeng, J., Lyon-Caen, H., Bollinger, L., Galetzka, J., Genrich, J., Thomas, M., Chanard, K., Sapkota, S.N., Raujari, S., Shrestha, P., Ding, L., Flouzat, M., 2012. Convergence rate across the Nepal Himalaya and interseismic

decoupling on the main Himalayan thrust: implications for seismic hazard. J. Geophys. Res. 117, B044403. http://dx.doi.org/10.1029/2011JB009071.
Adhikari, L.B., Gautam, U.P., Koirala, B.P., M Bhattarai, B.P., Kandel, T., Gupta, R.M., Timsina, C., Maharjan, N., Maharjan, K., Dahal, T., Hoste-Colomer, P., Cano, Y., Dandine, M., Guilhem, A., Merrer, S., Roudil, S.P., Bollinger, L., December, 2015. The aftershock sequence of the 2015 April 25 Gorkha–Nepal earthquake. Geophys. J. Int. 203 (3), 2119–2124. http://dx.doi.org/10.1093/gji/ggv412.
Allmann, B.P., Shearer, P.M., 2009. Global variations of stress drop for moderate to large earthquakes. Geophys. J. Int. 114, B01310. http://dx.doi.org/10.1029/2008JB005821.
Alsdorf, D., Brown, L., Nelson, D., Ross, A., Makovsky, Y., Klemperer, S., Zhao, W., 1998. Crustal deformation of the Lhasa Terrane, Tibet plateau from INDEPTH seismic reflection profiles. Tectonics 17 (4), 501–519.
Ambraseys, N.N., Douglas, J., 2004. Magnitude calibration of north indian earthquakes. Geophys. J. Int. 158, 1–42. http://dx.doi.org/10.1111/j.1365-246X.2004.02323.
Ambraseys, N., Jackson, D., 2003. A note on early earthquakes in northern India and southern Tibet. Curr. Sci. 84, 570–582.
Mahadevan, I., Bendick, R., Liang, H., 2010. Why subduction zones are curved. Tectonics 29, TC6002. http://dx.doi.org/10.1029/2010TC002720.
Avouac, J.-P., 2003. Mountain building, erosion, and the seismic cycle in the Nepal Himalaya. Adv. Geophys. 46, 1–80.
Avouac, J.-P., 2015. From geodetic imaging of seismic and aseismic slip to dynamic modeling of the seismic cycle. Annu. Rev. Earth Planet Sci. 43, 8.1–8.39.
Avouac, J.-P., Meng, L., Wei, S., Wang, T., Ampuero, J.-P., 2015. Lower edge of locked main Himalayan thrust unzipped by the 2015 Gorkha earthquake. Nat. Geosci. http://dx.doi.org/10.1038/NGEO2518.
Banerjee, P., Bürgmann, R., Nagarajan, B., Apel, E., 2008. Intraplate deformation of the Indian subcontinent. Geophys. Res. Lett. 35, L18301. http://dx.doi.org/10.1029/2008GL035468.
Bashyal, R.P., 1998. Petroleum exploration in Nepal. J. Nepal Geol. Soc. 18, 19–24.
Bendick, R., Bilham, R., 2001. How perfect is the Himalayan arc? Geology 29, 791–794.
Berger, A.F., Jouanne, F., Hassini, F., Mugnier, J.L., 2004. Modelling the spatial distribution of present-day deformation in Nepal: how cylindrical is the Main Himalayan Thrust in Nepal? Geophys. J. Int. 156, 94–114. http://dx.doi.org/10.1111/j.1365-246X.2004.02038.x.
Bilham, R., 1995. Location and magnitude of the 1833 Nepal earthquake and its relation to the rupture zones of contiguous great Himalayan earthquakes. Curr. Sci. 69 (2), 155–187.
Bilham, R., 2001. Slow tilt reversal of the Lesser Himalaya between 1862 and 1992 at 78°E, and bounds to the southeast rupture of the 1905 Kangra earthquake. Geophys. J. Int. 144, 1–23.
Bilham, R., 2004. Earthquakes in India and the Himalaya: tectonics, geodesy and history. Ann. Geophys. 47 (2), 839–858.
Bilham, R., 2015. Raising Kathmandu. Nat. Geosci. 8, 582–584.
Bilham, R., 2016. The Gorkha earthquake and the Tehri dam. Nepal Eng. Assoc. Tech. J. 1–14.
Bilham, R., Wallace, K., 2005. Future Mw>8 earthquakes in the Himalaya: implications from the 26 Dec 2004 Mw=9.0 earthquake on India's eastern plate margin. Geol. Surv. India Spec. Publ. 85, 1–14.
Blanpeid, M.L., Lockner, D.A., Byerlee, J.D., 1995. Frictional slip of granite at hydrothermal conditions. J. Geophys. Res. 100, 13045–13064.
Bollinger, L., Tapponier, P., Sapkota, S.N., Klinger, Y., 2015. Slip deficit in central Nepal: omen for a repeat of the 1344 AD earthquake. Earth, Planets Space. http://dx.doi.org/10.1186/s40623-016-0489-1.
Bollinger, L., Sapkota, S.N., Tapponnier, P., Klinger, Y., Rizza, M., Van der Woerd, J., Tiwari, D.R., Pandey, R., Bitri, A., Bes de Berc, S., 2014. Estimating the return times of great Himalayan earthquakes in eastern Nepal: evidence from the Patu and Bardibas strands of the main frontal thrust. J. Geophys. Res. Solid Earth 119. http://dx.doi.org/10.1002/2014JB010970.
Bomford, G., 1928. Three sources of error in precise leveling. Surv. India Prof. Pap. 22, 40.
Borkar, Y., Kumar, A., Gupta, S.C., Kumar, Arjun, 2013. Source parameters and scaling relation for local earthquakes in the Garwhal and Kumaon Himalaya, India. Int. J. Adv. Seismol. 1, 1–15.
Burgette, R.J., Weldon II, R.J., Schmidt, D.A., 2009. INterseismic uplift rates for western Oregon and along-strike variation in locking on the Cascadia subduction zone. J. Geophys. Res. Solid Earth 114, B01408. http://dx.doi.org/10.1029/2008JB005679.
Bürgmann, R., Kogan, M.G., Steblov, G.M., Hilley, G., Levin, V.E., Apel, T., 2005. Interseismic decoupling and asperity distribution along the Kamchatka subduction zone. J. Geophys. Res. Solid Earth 110. http://dx.doi.org/10.1029/2005JB003648.
Caldwell, W.B., Klemperer, S.L., Lawrence, J.F., Rai, S.S., Ashish, 2013. Characterizing the main Himalayan thrust in the Garhwal Himalaya, India with receiver function CCP stacking. Earth Planet. Sci. Lett. 367, 15–27. http://dx.doi.org/10.1016/j.epsl.2013.02.009.
Chen, W.-P., Molnar, P., 1977. Seismic moments of major earthquakes and the average rate of slip in Central Asia. J. Geophys. Res. Solid Earth 82, 2945–2969.
Chen, W.-P., Molnar, P., 1983. Focal depths of intracontinental and intraplate earthquakes and their implications for the thermal and mechanical properties of the lithosphere. J. Geophys. Res. Solid Earth 88, 4183–4214.
Chlieh, M., Avouac, J.-P., Sieh, K., Natawidjaja, D.H., Galetzka, J., 2008. Heterogeneous coupling of the Sumatran megathrust constrained by geodetic and paleogeodetic measurements. J. Geophys. Res. Solid Earth 113, B05305. http://dx.doi.org/10.1029/2007JB004981.
Chugh, R.S., 1974. Study of recent crustal movements in India and future programs. In: International Symposium on Recent Crustal Movements, Zurich.
Cotton, F., Campillo, M., Deschamps, A., Rastogi, B.K., 1996. Rupture history and seismotectonics of the 1991 Uttarkashi, Himalaya earthquake. Tectonophysics 258, 35–51.
Dasgupta, S., Mukhopadhyay, B., 2014. Earthquake in Garhwal Himalaya - archival materials with commentary. Indian J. Hist. Sci. 41.1, 21–33.
Denolle, M.A., Fan, W., Shearer, P.M., 2015. Dynamics of the 2015 M7.8 Nepal earthquake. Geophys. Res. Lett. 42, 7467–7475. http://dx.doi.org/10.1002/2015GL065336.
Dreger, D., Nadeau, R.M., Chung, A., 2007. Repeating earthquake finite source models: strong asperities revealed on the San Andreas Fault. Geophys. Res. Lett. 34, L23302 doi:101029/2007GL031353.
Duputel, Z., Vergne, J., Rivera, L., Wittlinger, G., Farra, V., Hetényi, G., 2016. The 2015 Gorkha earthquake: a large event illuminating the Main Himalayan Thrust fault. Geophys. Res. Lett. 43 http://dx.doi.org/10.1002/2016GL068083.
Elliott, J.R., Jolivet, R., Gonzalez, P., Avouac, J.-P., Hollingsworth, J., Searle, M., Stevens, V., 2016. Himalayan megathrust geometry and relation to topography revealed by the Gorkha earthquake. Nat. Geosci. 9, 174–180. http://dx.doi.org/10.1038/NGEO2623.
Engdahl, E.R., Villaseñor, A., 2002. Global seismicity: 1900–1999. In: Lee, W.H.K., Kanamori, H., Jennings, P.C., Kisslinger, C. (Eds.), International Handbook of Earthquake and Engineering Seismology, Part A, Chapter 41. Academic Press, pp. 665–690.
Feldl, N., Bilham, R., 2006. Great Himalayan earthquakes and the Tibetan plateau. Nature 444, 165–170. http://dx.doi.org/10.1038/nature05199.
Gahalaut, V.K., Chander, R., 1992. On the active tectonics of the Dehra Dun region from observations of ground elevation changes. J. Geol. Soc. India 39, 61–68.
Gahalaut, V.K., Chander, R., 1997. Evidence for an earthquake cycle in NW Outer Himalaya near 78°E longitude from precision levelling observations. Geophys. Res. Lett. 24, 225–228.
Gahalaut, V.K., Chander, R., 1999. Geodetic evidence for accumulation of earthquake generating strains in the NW Himalaya near 75.5°E longitude. Bull. Seismol. Soc. Am. 89, pp.837–843.
Gahalaut, V.K., Gupta, P.K., Chander, R., Gaur, V.K., 1994. Minimum norm inversion of observed ground elevation changes for slips on the causative fault during the 1905 Kangra earthquake. Proc. Indian Acad. Sci. - Earth Planet. Sci. 103, 401–411.
Galetzka, J., Melgar, D., Genrich, J., Geng, J., Owen, S., Lindsey, E., Xu, X., Bock, Y., Avouac, J.-P., Adhikari, L., Upreti, B., Pratt-Sitaula, B., Bhattarai, T., Sitaula, B., Moore, A., Hudnut, K., Szeliga, W., Normandeau, J., Fend, M., Flouzat, M., Bollinger, L., Shrestha, P., Koirala, B., Gautam, U., Bhatterai, M., Gupta, R., Kandel, T., Timsina, C., Sapkota, S., Rajaure, S., Maharjan, N., 2015. Slip pulse and resonance of the Kathmandu basin during the 2015 Gorkha earthquake. Nepal, Sci. 349, 1091.
Gavillot, Y., Meigs, A., Yule, D., Hemance, R., Rittenour, T., Madugo, C., Malik, M., 2016. Shortening rate and Holocene rupture on the Riasi fault system in the Kashmir Himalaya: active wedge thrusting within the NW Himalayan orogenic wedge. Bull. Geol. Soc. Am. B31281.1. http://dx.doi.org/10.1130/B31281.1.
Grandin, R., Vallée, M., Satriano, C., Lacassin, R., Klinger, Y., Simoes, M., Bollinger, L., 2015. Rupture process of the Mw =7.9 2015 Gorkha earthquake (Nepal): insights into 220 Himalayan megathrust segmentation. Geophys. Res. Lett. 42, 221. http://dx.doi.org/10.1002/2015GL066044.
Hardebeck, J.L., Aron, A., 2009. Earthquake stress drops and inferred fault strength on the Hayward fault, east san Francisco Bay, California. Bull. Seismol. Soc. Am. 99, 1801–1814. http://dx.doi.org/10.178/0120080242.
Hauck, M.L., Nelson, K.D., Brown, L.D., Zhao, W., Ross, A.R., 1998. Crustal structure of the Himalayan orogen at 90° east longitude from Project INDEPTH deep reflection profiles. Tectonics 17 (4), 481–500. http://dx.doi.org/10.1029/98TC01314.
Hayes, G.P., Barnhart, W., Briggs, R., Yeck, W., McNamara, D.E., Wald, D., Nealy, J., Benz, H., Gold, R., Jaiswal, K., Marano, K., Earle, P., Hearne, M., Smoczyk, G., Wald, L., Samsonov, S., 2015. Rapid characterization of the 2015 Mw 7.8 Nepal (Gorkha) earthquake. Seismol. Res. Lett. 86 (6), 1557–1567.
Herman, F., Copeland, P., Avouac, J.-P., Bollinger, L., Mahéo, G., Le Fort, P., Rai, S., Foster, D., Pêcher, A., Stüwe, K., Henry, P., 2010. Exhumation, crustal deformation, and thermal structure of the Nepal Himalaya derived from the inversion of thermochronological and thermobarometric data and modeling of the topography. J. Geophys. Res. 115, B06407. http://dx.doi.org/10.1029/2008JB006126.
Hetland, E.A., Simons, M., Dunham, E.M., 2010. Post seismic and interseismic fault creep I; Model description. Geophys. J. Int. 181, 81–98.
Hossler, T., Bollinger, T.L., Sapkota, S.N., Lavé, J., Gupta, R.M., Kandel, T.P., 2016. Surface ruptures of large Himalayan earthquakes in western Nepal: evidence along a reactivated strand of the main boundary thrust. Earth Planet. Sci. Lett. 434, 187–196.
Hubbard, J., Almeida, R., Foster, A., Sapkota, S., Burgi, P., Tapponnier, P., 2013. Structural segmentation controlled the 2015 Mw 7.8 Gorkha earthquake rupture in Nepal. Geology G38077.1. http://dx.doi.org/10.1130/G38077.1 first published on July 8, 2016.
Hyndman, R.D., 2013. Downdip landward limit of Cascadia great earthquake rupture. J. Geophys. Res. Solid Earth. 118 http://dx.doi.org/10.1002/jgrb.50390.
Jackson, M., Bilham, R., 1994. Constraints on Himalayan deformation inferred from vertical velocity fields in Nepal and Tibet. J. Geophys. Res. 99 (B7), 13897–13912.

Please cite this article in press as: Bilham, R., et al., Implications for elastic energy storage in the Himalaya from the Gorkha 2015 earthquake and other incomplete ruptures of the Main Himalayan Thrust, Quaternary International (2017), http://dx.doi.org/10.1016/j.quaint.2016.09.055

Jayangondaperumal, R., Wesnousky, S.G., Choudhuri, B.K., 2011. Near-surface expression of early to late Holocene displacement along the northeastern Himalayan frontal thrust at Marbang Korong Creek, Arunachal Pradesh, India. Bull. Seism. Soc. Amer 101 (6), 3060–3064.

Johnson, K.M., Mavrommatis, A., Segall, P., 2016. Small interseismic asperities and widespread aseismic creep on the northern Japan subduction interface. Geophys. Res. Lett. 43 http://dx.doi.org/10.1002/2015GL066707.

Jones, L., Molnar, P., 1979. Some characteristics of foreshocks and their possible relationship to earthquake prediction and premonitory slip on faults. J. Geophys. Res. 84, 3596–3608.

Joshi, A., 2006. Analysis of strong motion data of the Uttarkashi earthquake of 20th October 1991 and the Chamoli earthquake of 28th march 1999 for determining the q value and source parameters. ISET J. Earthq. Technol. 43, 11–29 paper 468.

Kaila, K., Tripathi, K., Dixit, M., 1984. Structure along Wular Lake-Gulmarg-Naoshera profile across Pir Panjal range of the Himalayas from deep seismic soundings. J. Geol. Soc. India 25 (11).

Kayal, J.R., 2001. Microearthquake activity in some parts of the Himalaya and the tectonic model. Tectonophysics 339, 331–351.

Kumar, S., Wesnousky, S.G., Rockwell, T.K., Briggs, R.W., Thakur, V.C., Jayangondaperumal, R., 2006. Palæoseismic evidence of great surface rupture earthquakes along the Indian Himalaya. J. Geophys. Res. 111, B03304. http://dx.doi.org/10.1029/2004JB003309.

Kumar, A., Singh, S.K., Mitra, S., Priestly, K., Dayal, S., 2017. The 2015 April 2015 Gorkha (Nepal) earthquakes and aftershocks: implications for lateral heterogeneity of the main Himalayan thrust. Geophys. J. Int. 208, 992–1008. http://dx.doi.org/10.1093/gji/ggw438.

Kumar, S., Wesnousky, S.G., Jayangondaperumal, R., Nakata, T., Kumahara, Y., Singh, V., 2010. Paleoseismological evidence of surface faulting along the northeastern Himalayan front, India: timing, size, and spatial extent of great earthquakes. J. Geophys. Res. 115, B12422. http://dx.doi.org/10.1029/2009JB006789.

Langbein, J., 2008. Noise in GPS displacement measurements from southern California and southern Nevada. J. Geophys. Res. 113, B05405. http://dx.doi.org/10.1029/2007JB005247.

Lavé, J., Avouac, J.-P., 2001. Fluvial incision and tectonic uplift across the Himalayas of cental Nepal. J. Geophys. Res. 106, 26561–26591.

Lavé, J., Yule, D., Sapkota, S., Basant, K., Madden, C., Attal, M., Pandey, R., 2005. Evidence for a great medieval earthquake (~1100 A.D.) in the central Himalayas, Nepal. Science 307, 1302–1305.

Lay, T., Ye, L., Koper, K., Kanamori, H., 2016. Assessment of teleseismically-determined source parameters for the April 25, 2015 M_W 7.9 Gorkha, Nepal earthquake and the May 12, 2015 M_W 7.2 aftershock. Tectonophysics. http://dx.doi.org/10.1016/j.tecto.2016.05.023.

Le Roux-Mallouf, R., Godard, V., Cattin, R., Ferry, M., Gyeltshen, J., Ritz, J.-F., Drupka, D., Guillou, V., Arnold, M., Aumaître, G., Bourlès, D.L., Keddadouche, K., 2015. Evidence for a wide and gently dipping Main Himalayan Thrust in western Bhutan. Geophys. Res. Lett. 42 http://dx.doi.org/10.1002/2015GL063767.

Lindsey, E., Natsuaki, R., Xu, X., Shimada, M., Hashimoto, H., Melgar, D., Sandwell, D., 2015. Line of sight deformation from ALOS-2Interferometry: Mw7.8 Gorkha earthquake and Mw 7.3 aftershock. Geophys. Res. Lett. 42, 6655–6661. http://dx.doi.org/10.1002/2015GL065385.

Lyon Caen, H., Molnar, P., 1985. Gravity-anomalies, flexure of the Indian plate, and the structure, support and evolution of the Himalaya and Ganga basin. Tectonics 4 (6), 513–538.

Mahesh, P., Gupta, S., Saikia, U., Rai, S.S., 2015. Seismotectonics ?and ?crustal ?stress fi?eld ?in ?the ?Kumaon–Garhwal ?Himalaya. Tectonophysics. http://dx.doi.org/10.1016/j.tecto.2015.05.016.

Malik, J.N., Sahoo, Ajit K., Shah, Afroz A., Shinde, Dattatraya P., Juyal, N., Singhvi, A.K., 2010. Paleoseismic evidence from trench investigation along Hajipur fault, Himalayan Frontal Thrust, NW Himalaya: implications of the faulting pattern on landscape evolution and seismic hazard. J. Struct. Geol. 32, 350–361.

Marone, C., 1998. Laboratory-derived friction laws and their application to seismic faulting. Ann. Rev. Earth Planet Sci. 26, 643–696.

Martin, S., Szeliga, W., 2010. A catalog of felt intensity data for 589 earthquakes in India, 1636-2009. Bull. Seismol. Soc. Am. 100, 536–569. http://dx.doi.org/10.1785/0120080328.

Mencin, D., Bendick, R., Upreti, B., Adhikari, D., Gajurel, A., Bhattarai, R., Shrestha, H., Bhattarai, T., Manandhar, N., Galetzka, J., Knappe, E., Pratt-Situala, B., Aoudia, A., Bilham, R., 2016. Himalayan strain reservoir inferred from limited afterslip following the Gorkha earthquake. Nat. Geosci. http://dx.doi.org/10.1038/ngeo2734.

Mishra, R.L., Singh, I., Pandey, A., Rao, P.S., Sahoo, H.K., Jayangondaperumal, R., 2016. Paleoseismic evidence of a giant medieval earthquake in the eastern Himalaya. Geophys. Res. Lett. 43 http://dx.doi.org/10.1002/2016GL068739.

Mitra, S., Priestley, K., Bhattacharyya, A.K., Gaur, V.K., 2005. Crustal structure and earthquake focal depths beneath northeastern India and southern Tibet. Geophys. J. Int. 160, 227–248. http://dx.doi.org/10.1111/j.1365-246X.2004.02470.x.

Molnar, P., 1990. A review of the seismicity and the rates of underthrusting and deformation at the Himalaya. J. Himal. Geol. 1 (2), 131–154.

Molnar, P., Deng, Q., 1984. Faulting associated with large earthquakes and the average rate of deformation in central and eastern Asia. J. Geophys. Res. 89, 6203–6227.

Molnar, P., England, P., 1990. Temperatures, heat flux, and frictional stress near major thrust faults. J. Geophys. Res. 95, 4833–4856.

Mugnier, J.L., Gajurel, A., Huyghe, P., Jayangondaperumal, R., Jouanne, F., Upreti, B., 2013. Structural interpretation of the great earthquakes of the last millennium in the central Himalaya. Earth-Science Rev. 127, 30–47.

Nábělek, J., Hetényi, G., Jérôme, V., Sapkota, S., Kafle, B., Jiang, M., Heping, S., Chen, J., Huang, B., 2009. Underplating in the Himalaya-Tibet collision zone revealed by the Hi-CLIMB experiment. Science 325, 1371–1374. http://dx.doi.org/10.1126/science.1167719.

Nakata, T., 1989. Active faults of the Himalaya of India and Nepal. In: Malinconico Jr., L.L., Lillie, R.J. (Eds.), Tectonics of the Western Himalayas, pp. 243–264. Geol. Soc. of Am. Spec. Pap. 232, Boulder, Colo.

Nakata, T., 1972. Geomorphic history and crustal movements of the foothills of the Himalayas. Sci. Rep. Tohoku Univ. 22, 39–177. Series 7.

Nakata, T., 1998. First successful paleoseismic trench study on active faults in the Himalaya. Eos Trans. AGU 79 (45). Fall Meet Suppl., Abstract S22A-18.

Ni, J., Barazangi, M., 1984. Seismotectonics of the Himalayan collision zone: geometry of the underthrusting Indian plate beneath the Himalaya. J. Geophys. Res. 89 (B2), 1147–1163. http://dx.doi.org/10.1029/JB089iB02p01147.

Philip, G., Suresh, N., Bhakuni, S.S., 2004. Active tectonics in the northwestern outer Himalaya: evidence of large-magnitude palaeoearthquakes in Pinjaur Dun and the Frontal Himalaya. Curr. Sci. 106, 211–222.

Rikitake, T., 1976. Earthquake Prediction. Elsevier, p. 357.

Rikitake, T., 1982. Earthquake Forecasting and Warning. Reidel, p. 402.

Ruff, L.J., 1999. Dynamic stress drop of recent earthquakes: variations within subduction zones. Pure Appl. Geophys. 154, 409–431. http://dx.doi.org/10.1007/s000240050237.

Sapkota, S.N., Bollinger, L., Klinger, Y., Tapponnier, P., Gaudemer, Y., Tiwari, D., 2013. Primary surface ruptures of the great Himalayan earthquakes in 1934 and 1255. Nat. Geosci. 6, 71–76.

Satyabala, S., Zhaohui Yang, P., Bilham, R., 2012. Stick-slip advance of the Kohat plateau Pakistan. Nat. Geosci. 5, 147–150. http://dx.doi.org/10.1038/ngeo1373.

Savage, J., 2006. Dislocation pileup as a representation of strain accumulation on a strike-slip fault. J. Geophys. Res. 111, B04405. http://dx.doi.org/10.1029/2005JB004021.

Schiffman, C., Bali, B.S., Szeliga, W., Bilham, R., 2013. Seismic slip deficit in the Kashmir Himalaya from GPS observations. Geophys. Res. Lett. 40, 5642–5645. http://dx.doi.org/10.1002/2013GL057700.

Scholz, C.H., 1982. Scaling laws for large earthquakes: consequences for physical models. Bull. Seism. Soc. Amer. 72, 1.

Scholz, C.H., 2002. The Mechanics of Earthquakes and Faulting. Cambridge University Press, p. 427.

Schulte-Pelkum, V., Monsalve, G., Sheehan, A., Pandey, M.R., Sapkota, S., Bilham, R., Wu, F., 2005. Imaging the indian subcontinent beneath the Himalaya. Nature 435, 1222–1225.

Schwartz, S.Y., Rokosky, J.M., 2007. Slow slip events and seismic tremor at circum-Pacific subduction zones. Rev. Geophys. 45 (3) http://dx.doi.org/10.1029/2006rg000208.

Seeber, L., Gornitz, V., 1983. River profiles along the Himalayan arc as indicators of active tectonics. Tectonophysics 92, 335–467.

Sharma, M.L., Wason, H.R., 1994. Occurrence of low stress drop earthquakes in the Garhwal Himalaya region. Phys. Earth Planet. Interiors 85, 265–272.

Shaw, B., Scholz, C.H., 2008. Slip length scaling in large earthqaukes: observatioons and theory and implications for earthquake physics. Geophys. Res. Lett. 28, 2995–2998. http://dx.doi.org/10.1029/2000GL012762.

Singh, S.K., Mohanty, W.K., Bansal, B.K., Roonwal, G.S., 2002. Ground motion in Delhi from future large/great earthquakes in the central seismic gap of the Himalayan arc. Bull. Seismol. Soc. Am. 92 (2), 555–569. http://dx.doi.org/10.1785/0120010139.

Stevens, V.L., Avouac, J.P., 2015. Interseismic decoupling of the main Himalayan thrust. Geophys. Res. Lett. 42, 5828–5837.

Stevens, V.L., Avouac, J.-P., 2016. Millenary Mw>9.0 earthquakes required by geodetic strain in the Himalaya. Geophys. Res. Lett. 43, 1118–1123. http://dx.doi.org/10.1002/2015GL067336.

Szeliga, W., Bilham, R., 2017. New constraints on the mechanism and rupture area for the M7.8 Kangra 1905 earthquake, NW Himalaya. Bull. Seism. Soc. Amer in press, 2017.

Szeliga, W., Hough, S.E., Martin, S., Bilham, R., 2010. Intensity, magnitude, location, and attenuation in India for felt earthquakes since 1762. Bull. Seismol. Soc. Am. 100, 570–584. http://dx.doi.org/10.1785/0120080329.

Thakur, V.C., Kumar, S., 2007. Seismotectonics of the 20 October 1991 Uttarkashi earthquake in Garhwal, Himalaya, north India. Terra Nova 6 (1), 90–94.

Tsuboi, C., 1933. Investigation of the deformation of the Earth's crust by precise geodetic means. Jpn. J. Astron. Geophys. 10, 93–248.

Upreti, B.N., Kumahara, Y., Nakata, T., 2007. Paleoseismological study in the Nepal Himalaya – present status. In: Proceedings of the Korea-Nepal Joint Symposium on Slope Stability and Landslides April, 1, 2007, pp. 1–9.

Vallée, M., 2013. Source time function properties indicate a strain drop independent of earthquake depth and magnitude. Nat. Commun. 4, 2606. http://dx.doi.org/10.1038/ncomms3606.

Vernant, P., Bilham, R., Szeliga, W., Drupka, D., Skalita, S., Bhattacharyya, A., Gaur, V.K., Pelgay, P., Cattin, R., Berthet, T., 2014. Clockwise rotation of the Brahmaputra valley: tectonic convergence in the eastern Himalaya, Naga Hills and Shillong plateau. J. Geophys. Res. 119 (8), 6558–6571. http://dx.doi.org/10.1002/2014JB011196.

Wallace, K., Bilham, R., Blume, F., Gaur, V.K., Gahalaut, V., 2005. Surface deformation in the region of the 1905 Kangra Mw = 7.8 earthquake in the period

Please cite this article in press as: Bilham, R., et al., Implications for elastic energy storage in the Himalaya from the Gorkha 2015 earthquake and other incomplete ruptures of the Main Himalayan Thrust, Quaternary International (2017), http://dx.doi.org/10.1016/j.quaint.2016.09.055

1846–2001. Geophys. Res. Lett. 32 (15), L15307. http://dx.doi.org/10.1029/2005GL02290.
Wang, K., Fialko, Y., 2015. Slip model of the 2015 Mw 7.8 Gorkha (Nepal) earthquake from inversions of ALOS-2 and GPS data. Geophys. Res. Lett. http://dx.doi.org/10.1002/2015GL065201.
Wesnousky, S.G., Kumar, S., Mohindra, R., Thakur, V.C., 1999. Uplift and convergence along the Himalayan frontal thrust of India. Tectonics 18, 967–976.
Wesnousky, S.G., Kumahara, Y., Chamlagain, D., Pierce, I., Karki, A., Gautam, D., 2016. Geological observations on large earthquakes along the Himalayan frontal fault near Kathmandu, Nepal. Earth Planet. Sci. Lett. 457, 366–375.
Williams, S.D.P., Bock, Y., Fang, P., Jamason, P., Nikolaidis, R.M., Prawirodirdjo, L., Miller, M., Johnson, D.J., 2004. Error analysis of continuous GPS time series. J. Geophys. Res. 109, B03412. http://dx.doi.org/10.1029/2003JB002741.
Xu, W., Bürgmann, R., Li, Z., 2016. An improved geodetic source model for the 1999 Mw 6.3 Chamoli earthquake, India. Geophys. J. Int. 205 (1), 236–242. http://dx.doi.org/10.1093/gji/ggw016.
Yeats, R.S., Nakata, T., Faraj, A., Fort, M., Mirza, M.A., Pandey, M.R., Stein, R.S., 1992. The Himalayan frontal fault system. Ann. Tect. 6, 85–98.
Yule, D., Dawson, S., Lavé, J., Tiwari, D., 2007. Possible evidence for surface rupture of the Main Frontal Thrust during the great 1505 Himalayan earthquake, far western Nepal. In: International Workshop on Investigation of Past Earthquakes in Nepal Himalaya, Kathmandu, Nepal.

Please cite this article in press as: Bilham, R., et al., Implications for elastic energy storage in the Himalaya from the Gorkha 2015 earthquake and other incomplete ruptures of the Main Himalayan Thrust, Quaternary International (2017), http://dx.doi.org/10.1016/j.quaint.2016.09.055